Li *et al. Satellite Navigation* (2022) 3:28
https://doi.org/10.1186/s43020-022-00089-9

Satellite Navigation
https://satellite-navigation.springeropen.com/

REVIEW

Open Access

Review of PPP–RTK: achievements, challenges, and opportunities

Xingxing Li[1], Jiaxin Huang[2], Xin Li[1*], Zhiheng Shen[1], Junjie Han[1], Linyang Li[1] and Bo Wang[3]

Abstract

The PPP–RTK method, which combines the concepts of Precise of Point Positioning (PPP) and Real-Time Kinematic (RTK), is proposed to provide a centimeter-accuracy positioning service for an unlimited number of users. Recently, the PPP–RTK technique is becoming a promising tool for emerging applications such as autonomous vehicles and unmanned logistics as it has several advantages including high precision, full flexibility, and good privacy. This paper gives a detailed review of PPP–RTK focusing on its implementation methods, recent achievements as well as challenges and opportunities. Firstly, the fundamental approach to implement PPP–RTK is described and an overview of the research on key techniques, such as Uncalibrated Phase Delay (UPD) estimation, precise atmospheric correction retrieval and modeling, and fast PPP ambiguity resolution, is given. Then, the recent efforts and progress are addressed, such as improving the performance of PPP–RTK by combining multi-GNSS and multi-frequency observations, single-frequency PPP–RTK for low-cost devices, and PPP–RTK for vehicle navigation. Also, the system construction and applications based on the PPP–RTK method are summarized. Moreover, the main issues that impact PPP–RTK performance are highlighted, including signal occlusion in complex urban areas and atmosphere modeling in extreme weather events. The new opportunities brought by the rapid development of low-cost markets, multiple sensors, and new-generation Low Earth Orbit (LEO) navigation constellation are also discussed. Finally, the paper concludes with some comments and the prospects for future research.

Keywords: PPP–RTK, Ambiguity resolution, Multi-GNSS, Smart device, Multi-sensor fusion

Introduction

At present, there is a significant increase in the demand for real-time precise positioning to support emerging applications including self-driving cars, unmanned aerial vehicles and smart device navigation. Two well-known techniques of Global Navigation Satellite System (GNSS), named Real-Time Kinematic (RTK) (Hofmann-Wellenhof et al., 2001; Rizos, 2002) and Precise Point Positioning (PPP) (Zumberge et al., 1997), have been widely applied in many areas for precise positioning. A real-time centimeter-accuracy positioning can be achieved by RTK through the double-difference Ambiguity Resolution (AR). However, the performance of RTK highly relies on communication links and short range to a reference station, which naturally leads to a huge communication burden and a lack of flexibility. By contrast, PPP is capable to obtain high-precision positions by using a single GNSS receiver but requires a long convergence time of 15–30 min (Collins 2008; Laurichesse et al., 2009).

To take full advantages of PPP and RTK and overcome the limitations of both techniques, a new method called PPP–RTK is proposed to perform rapid single-receiver ambiguity resolution by applying the precise corrections derived from a ground reference network (Wübbena et al., 2005). PPP–RTK can be regarded as an extension of the PPP model, which enables users to achieve absolute positioning using a single receiver with higher accuracy and faster convergence speed by applying ambiguity resolution. Unlike the Observable Space Representation

*Correspondence: xinli@sgg.whu.edu.cn

[1] School of Geodesy and Geomatics, Wuhan University, 129 Luoyu Road, Wuhan 430079, Hubei, China
Full list of author information is available at the end of the article

(OSR) correction adopted by RTK, which is the range corrections formulated by the lump sum of all GNSS-related errors, the corrections of PPP–RTK are given in the form of State Space Representation (SSR), providing various individual corrections such as for precise satellite orbit and clock, ionospheric and tropospheric delays, and Uncalibrated Phase Delay (UPD). The SSR corrections significantly reduce the communication burden and thereby are capable to support massive users (Li et al., 2011, 2014). In addition, the GNSS-related errors of different temporal and spatial characteristics can be represented separately, leading to possible improvements in positioning performance. In this sense, PPP–RTK can achieve the same accuracy and performance as RTK but with a wider operation range, lower communication burden, and higher robustness against errors, which is well considered as a prospective technology for emerging mass market and vehicular applications (Fig. 1).

Over the last decade, various PPP–RTK models were developed and their positioning performances were investigated (Geng et al., 2011; Li et al., 2011; Teunissen et al., 2010). Teunissen et al. (2010) developed a PPP–RTK model where the reparametrized network parameters, such as satellite and receiver clocks, phase and code delays, ambiguities, and atmospheric delays, are derived and taken as the corrections of observations for the users to enable ambiguity resolution. Considering that the network processing is time-consuming and hard to achieve in large-scale networks, a new PPP–RTK model was developed using a multilayer processing scheme to derive undifferenced augmentation corrections (Li et al., 2011, 2014). The precise orbit, satellite clock, phase bias, and atmospheric corrections are generated consecutively at the undifferenced level. The precise products at one layer will facilitate the corrections derivation at the next layer. Numerous studies demonstrated that PPP–RTK can achieve instantaneous ambiguity resolution and obtain centimeter-accuracy positioning results by using the augmentation corrections from regional reference networks. For better positioning performance, the research on bias estimation, atmospheric correction modeling, and rapid ambiguity resolution were conducted (Li et al., 2020a; Nadarajah et al., 2018; Wang et al., 2020b). With the advancement of multi-GNSS, the research of PPP–RTK experienced the developments from an ionosphere-free model to an undifferenced and uncombined model (Li et al., 2014; Odijk et al., 2016; Zhang et al., 2018a), single system to multi-system (Khodabandeh & Teunissen, 2016; Li et al., 2021a; Ma et al., 2020), and dual-frequency to multi-frequency (Li et al., 2022d; Psychas et al., 2021). Following the advancement of the theoretical study, the PPP–RTK service systems have been developed by several research institutions and commercial companies to provide real-time precise positioning services around the world. Nevertheless, there are still many challenges regarding the environmental effects and the algorithm

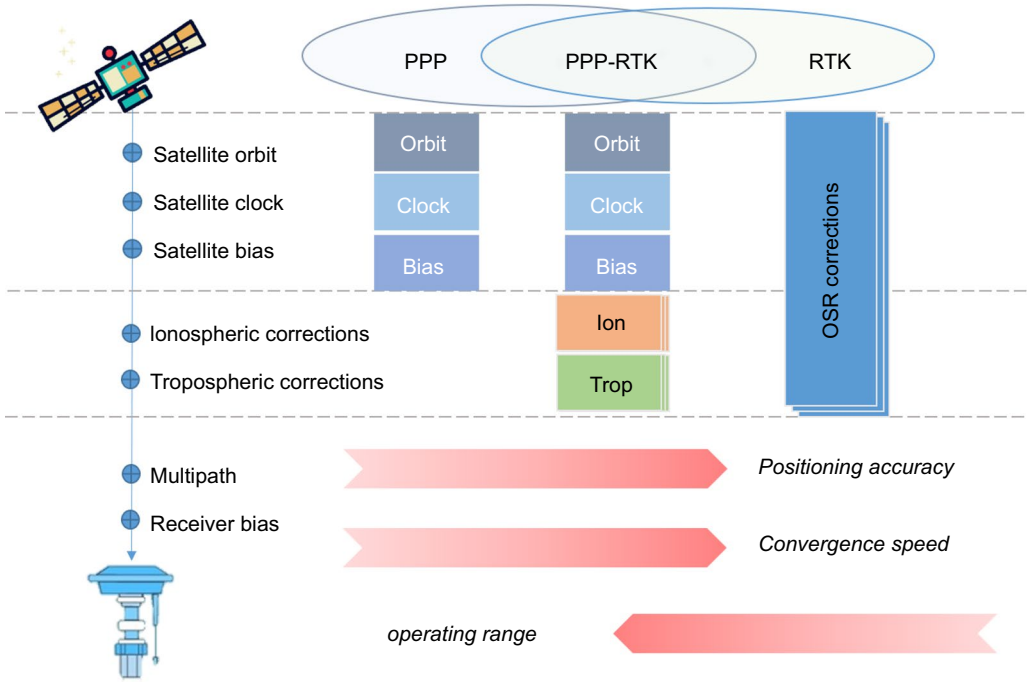

Fig. 1 Comparison of PPP, RTK, and PPP-RTK

development which restrict the wider application areas of PPP–RTK.

In this paper, we describe in detail the past research work on PPP–RTK and the future focus of the work with emphasis on the following aspects:

- to describe the fundamental approach to implement PPP–RTK and give an overview of the research on key techniques in a PPP–RTK system such as UPD estimation, precise atmospheric correction retrieval and modeling, and fast PPP ambiguity resolution.
- to summarize the system construction and commercial applications based on the PPP–RTK method.
- to overview the recent efforts and progress of PPP–RTK technique, including multi-frequency and multi-GNSS PPP–RTK, low-cost PPP–RTK using single-frequency observations, and PPP–RTK in real-time vehicle navigation.
- to discuss the major challenges and the future opportunities of PPP–RTK.

The remainder of this paper is organized as follows. Section 2 introduces the methods of PPP–RTK on both server and user ends. Section 3 describes the current PPP–RTK service systems built by the governments and commercial companies. After that, we summarize the literature on the major achievements of PPP–RTK, and finally discuss the challenges and opportunities in PPP–RTK focusing on future research outlook.

Methods of PPP–RTK

Since the concept of PPP–RTK was first proposed by Wübbena et al. (2005), many researchers implemented the PPP–RTK method and carried out several experimental verifications (Li et al., 2011, 2014; Oliveira et al. 2017; Psychas et al., 2021; Teunissen et al., 2010; Zhang et al., 2022). The flow of PPP–RTK generally goes through two major phases: the server phase which is to derive the precise orbit, clock, UPD, and atmospheric corrections based on the observations at network stations, and the user phase, where the corrections derived from network enable the fast AR of absolute positioning. The general flow of a PPP–RTK system is shown in Fig. 2. In this section, we will introduce the implementation method of PPP–RTK in detail from the server phase and the user phase. It will start with an overview of real-time precise orbit and clock products, then the general method of UPD estimation, precise atmospheric correction retrieval and modeling will be introduced. Finally, the rapid ambiguity resolution method with the precise atmospheric constraint will be described.

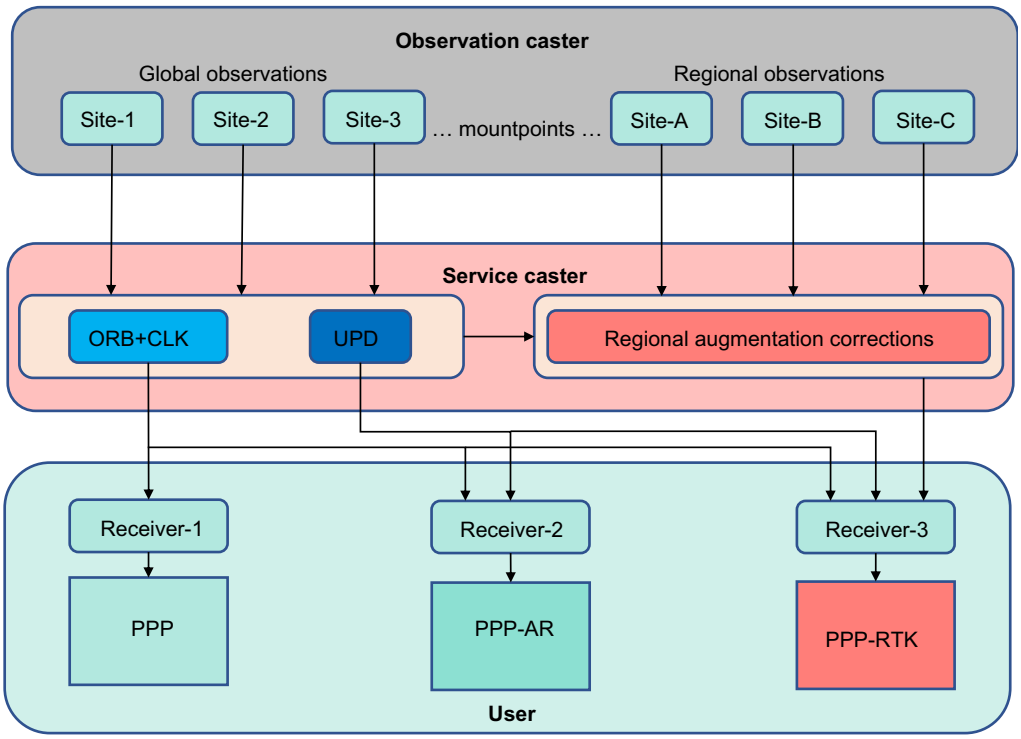

Fig. 2 General flow of a PPP-RTK system (ORB and CLK refer to precise satellite orbit and clock corrections, respectively)

Real-time precise orbit and clock products

Real-time precise orbit and clock products are the prerequisites for real-time and high-precision positioning, which are currently available on Real-Time Service (RTS), a Real-Time Pilot Project (RTPP) under the International GNSS Service (IGS) Real-Time Working Group (RTWG) since 2007 (https://igs.org/rts/products/). The RTWG was launched in 2001 with the aim at providing open data, open products, and open standards to real-time GNSS users (http://www.igs.org/rts). By the end of 2021, RTWG maintains over 200 multi-GNSS real-time reference stations, providing multi-GNSS real-time products such as orbit, clock, bias, etc. The technical content of the RTS products of each individual analysis center is presented in Table 1. GLONASS in Table 1 is Russian GLObal NAvigation Satellite System, Galileo is Europe's Galileo navigation satellite system, BDS is Chinese BeiDou Navigation Satellite System, QZSS is Japanese Quasi-Zenith Satellite System. The recent evaluation result of Li et al. (2022a) indicates that the real-time GNSS products provided by these analysis centers have good quality with the orbit errors of less than 5 cm and clock accuracy better than 0.15 ns.

Estimation of UPD products

The UPD products are generated in the server first for the subsequent ambiguity resolution. Affected by the ionospheric delays and residual model errors, the accuracy of undifferenced float ambiguity is not enough for the direct estimation of UPDs. Therefore, the UPD is generally estimated in the forms of Wide-Lane (WL) and Narrow-Lane (NL) combinations with the float ambiguities derived from reference networks (Ge et al., 2008; Li & Zhang, 2012). Assuming that there is a network of n stations and each station can observe m satellites, the relationship between UPDs and undifferenced float ambiguities is described as follows:

$$\begin{bmatrix} \tilde{\mathbf{N}}_1 \\ \tilde{\mathbf{N}}_2 \\ \vdots \\ \tilde{\mathbf{N}}_n \end{bmatrix} = \begin{bmatrix} \mathbf{I} & \cdots & \mathbf{O} & \mathbf{O} & \mathbf{R}_1 & \mathbf{S}_1 \\ \vdots & \ddots & \cdots & \mathbf{O} & \mathbf{R}_2 & \mathbf{S}_2 \\ \mathbf{O} & \vdots & \mathbf{I} & \vdots & \vdots & \vdots \\ \mathbf{O} & \mathbf{O} & \cdots & \mathbf{I} & \mathbf{R}_n & \mathbf{S}_n \end{bmatrix} \cdot \begin{bmatrix} \mathbf{N}_1 \\ \mathbf{N}_2 \\ \vdots \\ \mathbf{N}_n \\ \mathbf{U}_r \\ \mathbf{U}^s \end{bmatrix} \tag{1}$$

where $\tilde{\mathbf{N}}_i$ represents the float ambiguities at each station; $\mathbf{R}_i$ and $\mathbf{S}_i$ are the coefficient matrices for receiver and

Table 1 Real-time GNSS products of each analysis center

Analysis center	Name used GNSS	Products	Occurrence (s)
IGS	GPS + GLONASS + Galileo + BDS	Orbit	60
		Clock	5
ESA/ESOA (European Space Agency)	GPS	Orbit	5
		Clock	5
BKG (BundesamtfuerKartographie und Geodaesie)	GPS + GLONASS	Orbit	60
		Clock	5
		Code bias (GPS)	60
GMV (GMV Aerospace and Defense)	GPS + GLONASS + Galileo + BDS	Orbit	5
		Clock	5
		Code bias	5
CAS (Chinese Academy of Sciences)	GPS + GLONASS + Galileo + BDS + QZSS	Orbit	5
		Clock	5
		Code bias	10
GFZ (GeoForschungsZentrum Potsdam)	GPS + GLONASS + Galileo + BDS	Orbit	5
		Clock	5
		Code bias	5
CNES (Centre National d'Etudes Spatiales)	GPS + GLONASS + Galileo + BDS	Orbit	5
		Clock	5
		Code bias	5
		Phase bias	5
WHU (Wuhan University)	GPS + GLONASS + Galileo + BDS	Orbit	5
		Clock	5
DLR (Deutsches Zentrum fuer Luft-und Raumfahrt e.V)	GPS + GLONASS + Galileo + BDS + QZSS	Orbit	30
		Clock	5
		Code bias	30

satellite UPDs, respectively; $\mathbf{N}_i$ denotes the integer ambiguity vector at station i; $\mathbf{U}_r$ and $\mathbf{U}^s$ refer to the receiver- and satellite-specific UPDs, respectively. Provided that all integer ambiguities are exactly known, the UPDs can be estimated by the least-square method with one receiver or satellite UPD set as zero to eliminate the rank deficiency. Once the WL and NL UPDs are obtained, the raw UPDs on L1 and L2 frequency can be calculated according to Eq. (2), respectively:

$$\begin{cases} U_1 = U_{\mathrm{NL}} - \frac{f_2}{f_1 - f_2} \times U_{\mathrm{WL}} \\ U_2 = U_{\mathrm{NL}} - \frac{f_1}{f_1 - f_2} \times U_{\mathrm{WL}} \end{cases} \tag{2}$$

Another common way to estimate UPD is to develop a full-rank model based on S-system theory, where the re-parameterized UPDs can be obtained after achieving Double Difference (DD) ambiguity resolution in the network (Odijk et al., 2016; Teunissen & Khodabandeh, 2015; Zhang et al., 2011). In the network solution, the UPDs of receiver $U_{r,j}$ and satellite U_j^s on frequency j are reformed as:

$$\begin{cases} U_{r,j} = b_{r,j} - \frac{\mu_2 d_{r,1} - d_{r,2}}{\mu_2 - 1} + \frac{\mu_j}{\mu_2 - 1} d_{\mathrm{RDCB}} \\ U_j^s = b_j^s - \frac{\mu_2 d_1^s - d_2^s}{\mu_2 - 1} + \frac{\mu_j}{\mu_2 - 1} d_{\mathrm{SDCB}} \end{cases} \tag{3}$$

where $b_{r,j}$ and b_j^s denote the original frequency-dependent phase biases, while $d_{r,j}$ and b_j^s are those of their code counterparts; μ_j represents the coefficient of ionospheric delay on frequency j; d_{RDCB} and d_{SDCB} denote the receiver and satellite Differential Code Biases (DCBs), respectively. Khodabandeh and Teunissen (2018) inferred the impact of ambiguity resolution on the estimation of various parameters on the PPP–RTK server side. And it is proved from the mathematical model that receiver and satellite phase UPDs can benefit from the double-differenced AR in the network solution.

With the rapid development of satellite navigation systems, the UPD estimation model has been extended from a single-system to multi-system, and from the dual-frequency to the multi-frequency (Geng & Bock, 2013; Gu et al., 2015; Geng and Bock, 2016; Liu et al., 2017a, 2017b, 2017c; Li et al., 2018, 2019a). However, a variety of GNSS signals leads to a large amount of bias combination forms, which makes it difficult to apply the UPD corrections. In response to this circumstance, the approach of Observable-specific Signal Bias (OSB) parametrization was recently proposed, which enables each measurement to respond to individual bias correction (Deng et al. 2021; Li et al., 2022b; Villiger et al., 2019; Wang et al., 2020a).

In addition to the method of using UPDs to achieve Precise Point Positioning with Ambiguity Resolution (PPP-AR), Laurichesse and Mercier (2007) and Collins (2008) proposed two different PPP-AR methods, namely the Integer Recovery Clock (IRC) method and the decoupled satellite clock method. Even though the above methods are implemented in rather different ways, they are theoretically equivalent (Geng et al., 2010). Currently, some institutions such as CNES, Center for Orbit Determination in Europe (CODE) and Wuhan University have released their UPD or IRC products to global users (Banville et al., 2020; Hu et al., 2020). In addition, GREAT-UPD, the first open-source UPD estimation software, was also released in 2021 (Li et al., 2021b).

Precise atmospheric correction retrieval

The provision of accurate atmospheric delay corrections is crucial for improving the performance of precise positioning. For decades, several methods were proposed to retrieve high-accuracy atmospheric information. In this part, we will introduce the progress in tropospheric correction retrieval and ionospheric correction retrieval.

Tropospheric correction retrieval

There are two main methods for extracting tropospheric correction using ground-based GNSS technology: the double-difference network solution method and the PPP method (Bevis et al., 1992; Duan et al., 1996). The double-difference network solution method has high complexity and requires a long-distance to a reference station to determine the absolute tropospheric delay, which is not suitable for the PPP–RTK server to extract tropospheric corrections. Therefore, this section will focus on the tropospheric correction retrieval method based on the PPP model.

The GNSS raw code ($P_{r,j}^i$) and phase ($L_{r,j}^i$) observation equations can be written as following:

$$\begin{aligned} P_{r,j}^i &= \rho_r^i + t_r - t^i + I_{r,j}^i + m_{d,r}^i \times T_{d,r}^j + m_{w,r}^i \\ &\quad \times T_{w,r}^j + \left(d_{r,j} - d_j^i\right) + e_{r,j}^i \end{aligned} \tag{4}$$

$$\begin{aligned} L_{r,j}^i &= \rho_r^i + t_r - t^i - I_{r,j}^i + m_{d,r}^i \times T_{d,r}^j \\ &\quad + m_{w,r}^i \times T_{w,r}^j + \lambda_j \times N_{r,j}^i + \lambda \\ &\quad \times \left(b_{r,j} - b_j^i\right) + \varepsilon_{r,j}^i \end{aligned} \tag{5}$$

where the superscript i refers to satellite, and subscripts j, r refer to frequency and receiver, respectively; ρ_r^i denotes the geometric distance from the satellite to receiver; t_r and t^i represent the clock offset at receiver and satellite sides, respectively; $I_{r,j}^i$ is the ionospheric delay on frequency j; $T_{d,r}^i$ refers to the hydrostatic component of zenith tropospheric delay while $T_{w,r}^i$ is the wet

delay component; $m^i_{d,r}$ and $m^i_{w,r}$ are mapping function of the zenith hydrostatic delay and wet delay, respectively; λ_j is the wavelength of frequency j; $N^i_{r,j}$ refers to the integer ambiguity; $d_{r,j}$ and d^i_j are the pseudorange code biases of receiver and satellites, respectively, while $b_{r,j}$ and b^i_j are the counterparts in phase observations; $e^i_{r,j}$ and $\varepsilon^i_{r,j}$ denote the sum of measurement noise and unmodelled error for the code and carrier phase observations, respectively.

In the process of PPP solution, the hydrostatic delay part is usually corrected by a empirical model such as the Hopfield model (Hopfield, 1972) and Saastamoinen model (Saastamoinen 1972). While the wet delay part is treated as an unknown parameter to be estimated. Then the zenith tropospheric delay can be used directly or calculated as the slant tropospheric delay on the signal path by using the mapping function according to the needs. Several studies have demonstrated that higher accuracy can be obtained for tropospheric delay once carrier phase ambiguity is fixed to the integer (Li et al., 2014;). Therefore, in the PPP–RTK server, PPP-AR is generally applied at reference stations for atmospheric retrieval with precise satellite orbits, clocks, and UPDs.

In addition to the above method of directly estimating the zenith troposphere wet delay, there is another way to extract the slant wet delay using the Ionosphere-Free (IF) combined PPP. The code and phase IF observations can be defined as:

$$\begin{aligned} P^i_{r,\mathrm{IF}} &= \frac{f_1^2}{f_1^2-f_2^2}\times P^i_{r,1} - \frac{f_2^2}{f_1^2-f_2^2}\times P^i_{r,2} \\ &= \rho^i_r + t_r - t^i + m^i_{d,r}\times T^i_{d,r} + m^i_{w,r}\times T^i_{w,r} + \left(d_{r,\mathrm{IF}} - d^i_{\mathrm{IF}}\right) + e^i_{r,\mathrm{IF}} \\ L^i_{r,\mathrm{IF}} &= \frac{f_1^2}{f_1^2-f_2^2}\times L^i_{r,1} - \frac{f_2^2}{f_1^2-f_2^2}\times L^i_{r,2} \\ &= \rho^i_r + t_r - t^i + m^i_{d,r}\times T^i_{d,r} + m^i_{w,r}\times T^i_{w,r} + \lambda_{\mathrm{IF}}\times N^i_{r,\mathrm{IF}} + \lambda_{\mathrm{IF}}\times\left(b_{r,\mathrm{IF}} - b^i_{\mathrm{IF}}\right) + \varepsilon^i_{r,\mathrm{IF}} \end{aligned} \tag{6}$$

Here, the IF ambiguities can be recovered by resolving WL and NL ambiguities. Then, the slant tropospheric wet delay of each satellite at each station $T^i_{\mathrm{SW},r}$ can be derived from the IF phase observations as (Li et al., 2021a):

$$\begin{aligned} T^i_{\mathrm{SW,r}} =& L^i_{r,\mathrm{IF}} - \left(\rho^i_r + t_r - t^i + m^i_{d,r}\times T^i_{d,r}\right. \\ &\left. +\lambda_{\mathrm{IF}}\times N^i_{r,\mathrm{IF}} + \lambda_{\mathrm{IF}}\times\left(b_{r,\mathrm{IF}} - b^i_{\mathrm{IF}}\right)\right) \end{aligned} \tag{7}$$

We can see that extracting the slant tropospheric wet delay in this way can eliminate the error caused by the mapping function.

Ionospheric correction retrieval

The Carrier-to-Code Leveling (CCL) and PPP methods are the two commonly used ways to retrieve precise ionospheric delay (Ciraolo et al., 2007; Zhang & Li, 2012). However, the accuracy of the ionospheric delays derived with these two methods is affected by noise and multipath. Recently, the ambiguity resolution method is employed in PPP model for improving the accuracy of ionospheric delays, which is detailed in this section.

After the ambiguities are fixed correctly, all the estimable parameters in the IF combined PPP model are accurately known and taken as corrections in Eq. (8) to determine the ionospheric corrections of each satellite:

$$\begin{aligned} I^i_{r,j} =& \rho^i_r + t_r - t^i + m^i_{d,r}\times T^j_{d,r} \\ &+ m^i_{w,r}\times T^j_{w,r} \\ &+ \lambda_j\times N^i_{r,j} + \lambda\times\left(b_{r,j} - b^i_j\right) - L^i_{r,j} \end{aligned} \tag{8}$$

where integer ambiguities $N^i_{r,j}$ can be obtained based on WL and NL ambiguities. Likewise, the UPDs of each frequency are derived by WL and NL UPDs as Eq. (2).

For the uncombined PPP model, the ionospheric delay is processed as estimable parameters, which naturally adapts to the PPP–RTK processing since the estimated ionospheric delays can be taken as atmospheric corrections directly to augment the positioning performance (Li et al., 2013, 2021a; Ren et al., 2020)). In addition, the good expandability of the uncombined PPP model in a multi-GNSS condition also makes it more and more popular in GNSS data processing.

However, the ionospheric delay parameter is significantly correlated with satellite and receiver clock offsets, ambiguities as well as hardware delays. Generally, the ionospheric parameters in the PPP processing will absorb the code bias in the process of re-parameterization (Zhang et al., 2019). The re-parameterization can be written as:

$$I^i_r = I^i_{r,1} - \frac{f_2^2}{f_1^2-f_2^2}\times\left(d_{\mathrm{RDCB},12} + d^i_{\mathrm{SDCB},12}\right) \tag{9}$$

wherein the satellite DCBs can be corrected by the precise products, while the receiver DCBs can be estimated through a network solution (Zha et al., 2021). Note that the ionospheric delay derived from the PPP fixed solution is also biased by the phase delays. Fortunately, the biased ionospheric corrections can also work well for PPP–RTK users once a reasonable parameter estimation strategy is employed (Psychas & Verhagen, 2020).

Precise atmospheric delays modeling

Since the precise atmospheric corrections are calculated independently for each reference station, an interpolation method is employed to obtain the accurate corrections at a user station. The research on geospatially related parameter interpolation methods began as early as the emergence of RTK technology. Wanninger (1995) firstly introduced a Linear Interpolation Method (LIM). Then, the Linear Combination Method (LCM), Least Squares Collocation Method (LSCM), and Distance-based Linear Interpolation Method (DIM) were adopted for RTK corrections interpolation (Han 1997, Raquet, 1997; Gao et al., 1997). In addition to linear interpolation methods, Fotopoulos (2000) proposed a Lower-order Surface Model (LSM) for fitting spatially correlated parameters. The comprehensive assessments of these interpolation methods were conducted in several studies and their similar performance has been demonstrated (Al-Shaery et al., 2011; Dai et al., 2003; Wang et al., 2020b). These methods are generally applied to double-differenced modes in NRTK. For PPP–RTK processing, modifications should be made to adapt to the undifferenced atmospheric corrections. Therefore, Li et al. (2011) proposed a Modified Linear Combination Method (MLCM), which is expressed as:

$$\begin{bmatrix} 1 & 1 & \cdots & 1 \\ X_1 - X_u & X_2 - X_u & \cdots & X_n - X_u \\ Y_1 - Y_u & Y_2 - Y_u & \cdots & Y_n - Y_u \end{bmatrix} \cdot \begin{bmatrix} \alpha_1 \\ \alpha_2 \\ \vdots \\ \alpha_n \end{bmatrix} = \begin{bmatrix} 1 \\ 0 \\ 0 \end{bmatrix} \tag{10}$$

$$\sum_{i=1}^{n} \alpha_i = 1; \sum_{i=1}^{n} \alpha_i^2 = Min; \tilde{\nu}_u = \sum_{i=1}^{n} \alpha_i \times \tilde{\nu}_i \tag{11}$$

where X and Y are the station coordinates, subscript u denotes the user station; n is the total number of reference stations; α_i is the interpolation coefficient; $\tilde{\nu}_i$ refers to the atmospheric corrections at the reference stations while $\tilde{\nu}_u$ is those of the user station.

The above-mentioned interpolation method requires the server end to broadcast atmospheric corrections station by station, which makes it difficult to control the amount of data. To improve communication efficiency and ensure the privacy of the locations of reference stations, the grid-based atmosphere model of a polynomial function is becoming a promising tool for the regional atmospheric model (Cabinet Office, 2020). The generation of a grid-based atmosphere model consists of three steps. Firstly, the spacing between a reference point and grid node must be set in advance. Then, the atmosphere model can be generated through the polynomial fitting function using the atmospheric corrections extracted from all reference stations in the area. Taking a second-order polynomial fitting function as an example, it can be described as follows:

$$\begin{aligned} A_s =& C_{00} + C_{01} \times (\phi_s - \phi_0) \\ &+ C_{10} \times (\lambda_s - \lambda_0) + C_{11} \\ &\times (\phi_s - \phi_0) \times (\lambda_s - \lambda_0) \end{aligned} \tag{12}$$

where A_s is the atmospheric correction at a reference station; ϕ_s and λ_s represent the longitude and latitude of the reference station, respectively; while ϕ_0 and λ_0 are those of the center point of the area;C_{00}, C_{01}, C_{10} and C_{11} are the coefficients for the second-order polynomial. The polynomial coefficients of atmosphere can be estimated based on the least-square method. However, the polynomial model may not always fit well due to the uncertainties of atmosphere changes, especially when the operation area is expanded. Therefore, once the polynomial coefficients are obtained, a residual grid that represents the differences between the modeled and extracted values are further computed. In this way, the sum of polynomial fitting values and interpolated residuals from the surrounding grid nodes are the corrections users required.

Besides, there are also some atmospheric models which fully consider the spatio-temporal information of atmospheric delays. For tropospheric corrections, a second-order polynomial model which considers ellipsoid height was proposed and proven to improve the modeling accuracy in the case of large terrain fluctuations (Shi et al., 2014; Oliveira et al., 2017). In order to further expand the application area and balance between the accuracy and bandwidth. The Galileo High Accuracy Service (HAS) proposed a dual-layer Vertical Total Electron Content (VTEC) model to provide ionospheric corrections (Rovira-Garcia et al., 2021). Different from traditional models using a thin shell at a unique height, this model applies a 3D representation of the electron content distribution.

PPP rapid ambiguity resolution

Following the acquisition of the precise atmospheric corrections, the spatial atmosphere model will be used to provide accurate atmospheric delays to the users. Then, the corresponding ionospheric and tropospheric

corrections will then be imported into the PPP model in the form of virtual observations as:

$$\begin{cases} P_{r,j}^{i} = \rho_r^i + t_r - t^i + I_{r,j}^{i} + m_{d,r}^{i} \times T_{d,r}^{j} + m_{w,r}^{i} \times T_{w,r}^{j} + \left(d_{r,j} - d_j^i\right) + e_{r,j}^{i} \\ L_{r,j}^{i} = \rho_r^i + t_r - t^i - I_{r,j}^{i} + m_{d,r}^{i} \times T_{d,r}^{j} + m_{w,r}^{i} \times T_{w,r}^{j} + \lambda_j \times N_{r,j}^{i} + \lambda \times \left(b_{r,j} - b_j^i\right) + \varepsilon_{r,j}^{i} \\ l_{\mathrm{T}}^{i} = T_{r,j}^{i} - \hat{T}_m^i = \omega_{\mathrm{T}}, \omega_{\mathrm{T}} \sim N\left(0, \sigma_{\omega_{\mathrm{T}}}^2\right) \\ l_{\mathrm{I}}^{i} = I_{r,j}^{i} - \hat{I}_m^i = \omega_{\mathrm{I}}, \omega_{\mathrm{I}} \sim N\left(0, \sigma_{\omega_{\mathrm{I}}}^2\right) \end{cases} \tag{13}$$

where l_{T}^{i} and l_{I}^{i} are tropospheric and ionospheric constraints, respectively; $\hat{T}_m^i$ and $\hat{I}_m^i$ represent the precise tropospheric and ionospheric corrections, respectively; ω_{T} and ω_{I} are the differences between the corrections and the actual delays, which conform to the zero-mean white noise distribution. The variances of the corrections are mostly given as empirical values, such as 5 mm and 1 cm of ionospheric corrections for two small-scale networks with the average space of 20 km and 60 km in the research of Teunissen et al. (2010), whereas 10 cm and 14 cm were adopted in a 50 km spaced area (Zhang et al., 2011). For a proper stochastic model for a wide-area PPP–RTK, Zha et al. (2021) developed an ionosphere stochastic model which determines the variance according to the empirical distance exponent and the size of the reference network. Further, Li et al. (2022c) proposed a cross-validation method to assess the accuracy of the interpolated slant ionospheric corrections through the high temporal and spatial variation of ionospheric delays.

The above PPP model with external atmospheric constraints can effectively reduce the influence of atmospheric errors and accelerate the convergence of ambiguity resolution. For ambiguity resolution, a cascade ambiguity fixing strategy is commonly employed for uncombined PPP model, where the WL and L1 ambiguities are fixed step by step (Geng et al., 2020). For example, with broadcasted UPD products the WL ambiguities are fixed and then can be introduced to the PPP model as virtual observations for better estimation of L1 ambiguities. With these constraints, the accuracy of float L1 ambiguities will be improved and can be easily fixed by integer estimators. There are three well-known integer estimators including integer rounding (Dong & Bock, 1989), integer bootstrapping (Teunissen, 1998), and Least-squares Ambiguity Decorrelation Adjustment (LAMBDA, Teunissen, 1995). The last one is shown to be the optimal method by virtue of its maximum probability of correct integer estimation. To validate the ambiguity resolution, two indices known as bootstrapping success rate and ratio value are employed (Han, 1997). Moreover, with the increasing number of available satellites, a partial ambiguity resolution strategy is generally used for the multi-constellation ambiguity resolution (Teunissen 1999; Li et al., 2017a).

Parameter estimation and processing strategy at server and user

A PPP–RTK system contains two important parts, which are the server and the user (Teunissen & Khodabandeh, 2015). Due to their different functions, there are many differences in parameter estimation and data processing. On the server side, we focus on solving various errors and translating them into the products for broadcasting. These errors include tropospheric delays, ionospheric delays, satellite clocks as well as satellite phase and code biases. In order to facilitate the calculation, the coordinates of the reference station are usually fixed. While on the user side, we pay more attention to the positioning results. To obtain accurate positioning results quickly in the process of data processing, most of the errors mentioned on the server side are usually corrected or constrained by the products. Table 2 compares these parameters and their processing strategies between server and user sides.

Table 2 Comparison of important PPP-RTK parameters and processing strategies between server and user sides

Parameter	Notation and interpretation	Processing strategy	
		Server	User
Coordinates	$g_r^s(k) \cdot \Delta x_r^s(k), k = 1, 2, 3$	Fix	Estimate
ZTDs	$T_{w,r}^{i}$	Estimate	Constrain
Ionospheric delays	$\tilde{I}_{r,1}^{i} - \frac{f_2^2}{f_1^2 - f_2^2} \times \left(d_{\mathrm{RDCB},12} + d_{\mathrm{SDCB},12}^{i}\right)$	Estimate	Constrain
Satellite phase biases	$b_j^s - \frac{\mu_2 d_1^s - d_2^s}{\mu_2 - 1} + \frac{\mu_j}{\mu_2 - 1} d_{\mathrm{SDCB},12}$	Estimate	Correct
Satellite code biases	d_j^i	Correct	Correct

Table 3 Positioning performance of CLAS service

Positioning type	Positioning error	
	Horizontal	Vertical
Static	≤ 6 cm (95%) (3.47 cm (RMS))	≤ 12 cm (95%) (6.13 cm (RMS))
Kinematic	≤ 12 cm (95%) (6.94 cm (RMS))	≤ 24 cm (95%) (12.25 cm (RMS))

Systems and applications of PPP–RTK

Currently, the PPP–RTK method has been widely used in various applications. At the government level, Japan took the lead in establishing the Centimeter Level Augmentation Service (CLAS) based on the Quasi-Zenith Satellite System (QZSS). This system is committed to providing real-time PPP–RTK positioning services to the users across the country. The highly efficient atmospheric correction message, as well as the satellite orbit, clock, code bias, phase bias corrections of GPS, Galileo and QZSS satellites are broadcasted on the L6 frequency band to augment the positioning service. The performance indicators of CLAS are shown in Table 3 (https://qzss.go.jp/en/technical/ps-is-qzss/ps-is-qzss.html).

The new-generation BeiDou system also has the capability of providing PPP augmentation services (Yang et al., 2019). According to the related document published in 2020 (http://www.beidou.gov.cn/xt/gfxz/index_1.html), the BDS augmentation service which is called Precise Point Positioning Service will provide various augmentation corrections through PPP-B2b signal. The augmentation system shown in Fig. 3 is built in two steps. In the first step, the system will provide precise satellite corrections to wide-area users via GEO satellites to enable real-time PPP. In the second step, the regional augmentation corrections generated by the ground-based network will be provided to shorten the convergence time. At present, the system has completed the first step of construction, and can provide users with real-time decimeter-accuracy positioning services.

The Galileo PPP augmentation service is named High Accuracy Service (HAS) which aims at providing decimeter-accuracy PPP-AR service for global users and PPP–RTK service for European users(https://www.gsc-europa.eu/galileo/services/galileo-high-accuracy-service-has). The positioning augmentation corrections of HAS will be broadcasted through both satellite (Galileo E6-B signal) and the internet, aiming to achieve two service levels as shown in Table 4. The construction of the HAS system will be carried out in three steps including Phase 0 (HA testing and experimentation), Phase 1 (HA Initial Service) and Phase 2 (HA Full Service). At present, the HAS has completed the goal of Phase 0. According to the plan, the initial and full service will be provided in 2022 and 2024, respectively.

Moreover, several companies are also devoted to constructing commercial PPP–RTK systems, such as Trimble's CenterPoint-RTX Fast (https://positioningservices.trimble.com/services/rtx/centerpoint-rtx/), NovAtel's TerraStar-X (https://terrastar.net/services/terrastar-servi

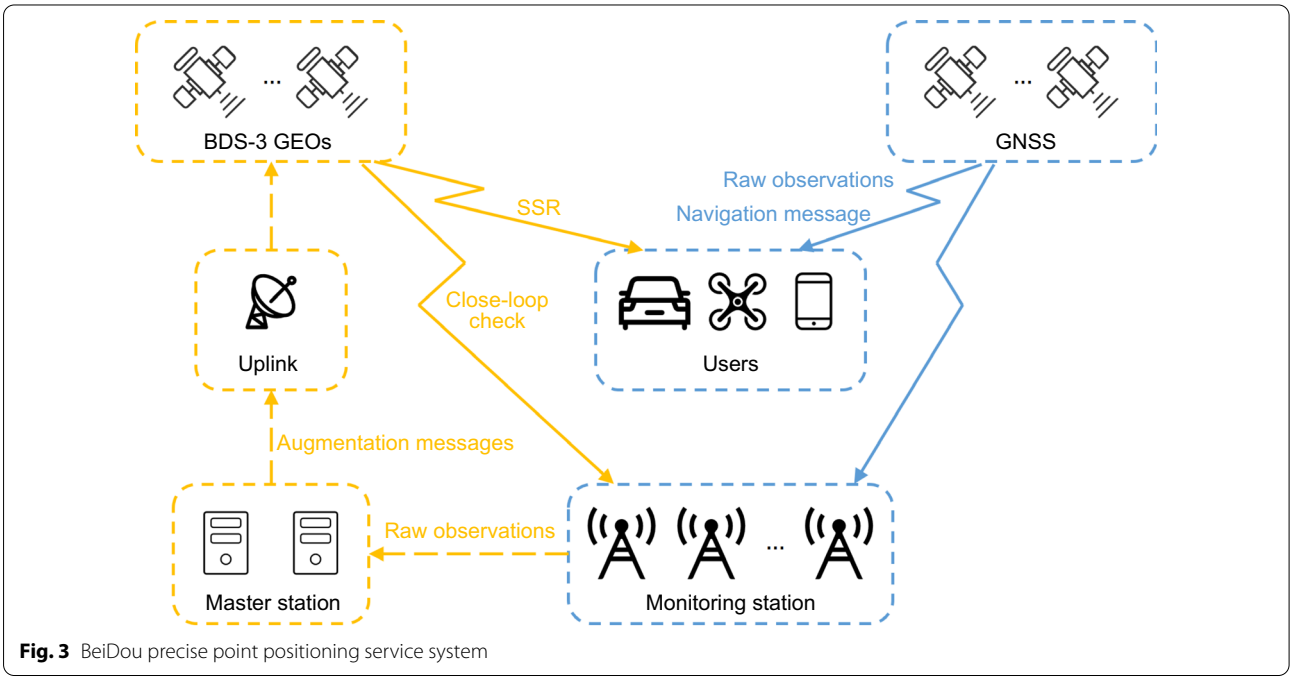

Fig. 3 BeiDou precise point positioning service system

Table 4 Target performances of HAS service

HAS	Service level I	Service level II
Coverage	Global	European Coverage Area
Corrections	Orbit, clock, biases	Orbit, clock, biases, ionospheric and tropospheric corrections
System	GPS + Galileo	GPS + Galileo
Frequencies	E1/E5a/E5b/E6; E5a + b; L1/L5; L2C	E1/E5a/E5b/E6; E5a + b; L1/L5; L2C
Horizontal accuracy (95%)	< 20 cm	< 20 cm
Vertical accuracy (95%)	< 40 cm	< 40 cm
Convergence time (s)	< 300	< 100
Availability (%)	99	99

ce-options), Ublox PointPerfect (https://www.u-blox.com/en/product/pointperfect), Qianxun XStar (https://www.qxwz.com/products/xingji), UniStrong Atlas (http://www.chinacm.org.cn/About.asp), Hi-Target Hi-RTP and so on. Trimble's CenterPoint-RTX Fast can reduce the PPP convergence time to less than 1 min in North America and Europe. TerraStar-X service provides GNSS corrections combined with OEM receivers from Hexagon and NovAtel. With these corrections, users can achieve fast convergence with centimeter-level accuracy. This service covers most of the USA and parts of southern Canada. PointPerfect is an advanced GNSS augmentation data service designed to achieve ultra-accurate, ultra-reliable, and immediately available positioning. The positioning results with 3–6 cm horizontal accuracy can be obtained within 30 s in the contiguous USA and Europe areas. Qianxun's XStar service mainly focuses on the Asia–Pacific region, providing users with precise location services with an availability rate higher than 99.99% and integrity better than 10^{-7}/h. The Atlas and Hi-RTP mainly provide high-precision augmentation services of centimeter accuracy in China and the surrounding areas. The comparison of these PPP–RTK services is listed in Table 5. These commercial PPP–RTK service systems can achieve centimeter-accuracy positioning within one minute. Thus, their application scope is no longer limited to the traditional markets like surveying and mapping but expanded to the emerging fields of navigation and positioning, such as robots, unmanned aircraft, and autonomous driving. Any kind of auto-guided machines will benefit from PPP–RTK service.

Achievements of PPP–RTK

PPP–RTK with multi-constellations

Currently, the world of satellite navigation is undergoing a dramatic change. With the full development of four major Global Navigation Satellite Systems (GPS, GLONASS, Galileo and BDS), there are over 120 available satellites for navigation and positioning. Furthermore, a variety of GNSS observations are available through the Multi-GNSS Experiment (MGEX) global network (Montenbruck et al., 2014, 2017; Rizos et al., 2013). The studies have demonstrated that satellite visibility, spatial geometry, convergence, accuracy, and reliability can be significantly improved with a combination of multi- constellations observations (Li et al., 2015, 2018).

Considering the significant benefits brought by multi-GNSS to the precise positioning, the multi-GNSS PPP–RTK is actively investigated in the recent years. Gu et al. (2015) assessed the performance of GPS + BDS PPP–RTK and demonstrated the benefits of multi-system fusion in shortening convergence time. A similar performance was also found in Wang and Li's research (Li et al., 2020a; Wang et al., 2020b). Nadarajah developed

Table 5 Commercial PPP-RTK service and performance (G, R, E, C represent GPS, GLONASS, Galileo, BDS respectively)

PPP-RTK service	Positioning error (RMS)		Convergence time (s)	System	Coverage
	Horizontal (cm)	Vertical (cm)			
CenterPoint-RTX	2	5	< 60	GR	North America and Europe
TerraStar-X	2	5	< 60	GRECJ	North America
PointPerfect	3–6	–	< 30	GRE	Europe and contiguous United States
XStar	2	–	< 50	GRECJ	Asia–Pacific
Atlas	4	–	–	–	Selected areas in China
Hi-RTP	3	5	< 60	GREC	Selected areas in China

a GPS + Galileo + BDS triple-system PPP–RTK model and evaluated its performance in multi-scale reference networks (Nadarajah et al., 2018). Zhang et al. (2021) implemented GLONASS PPP–RTK based on the Integer-Estimable Frequency Division Multiple Access (IE-FDMA, Teunissen, 2019) model, which fully considers the inter-frequency bias in heterogeneous network and enables rigorous integer ambiguity resolution of GLONASS. Thereafter, Ma et al. (2020) and Li et al. (2021a) expanded the model to the multi-GNSS one to achieve instantaneous centimeter-accuracy positioning. These results demonstrated the benefit of fusing multi-constellation observations in speeding convergence time, ambiguity fixing percentage, and positioning accuracy especially when the observation conditions are limited. The fixing percentages of AR for different combinations are compared under different cut-off elevation angles and presented in Fig. 4. The results show that compared with single-system PPP–RTK, multi-system PPP–RTK can significantly improve the success rate of AR and make the positioning result more stable even when the elevation angle is over 30°.

With the multi-constellation observations, some scholars further studied the PPP–RTK positioning performance in the case of larger-scale reference networks. Li et al. (2020d) evaluated the GPS + BDS PPP–RTK in Europe. The average distance between a user and reference stations is about 371 km. The results showed that ambiguity resolution can be achieved in almost 1 epoch, and the positioning accuracy was better than 1 cm and 3 cm for horizontal and vertical components, respectively. Another set of Australian experimental results also showed that PPP–RTK can achieve instantaneous ambiguity resolution in a reference network with a scale of 200–300 km (Li et al., 2021a). The above results indicate that PPP–RTK can achieve high-precision positioning over a broader operational range than the RTK approach, which also makes it have wider application prospects.

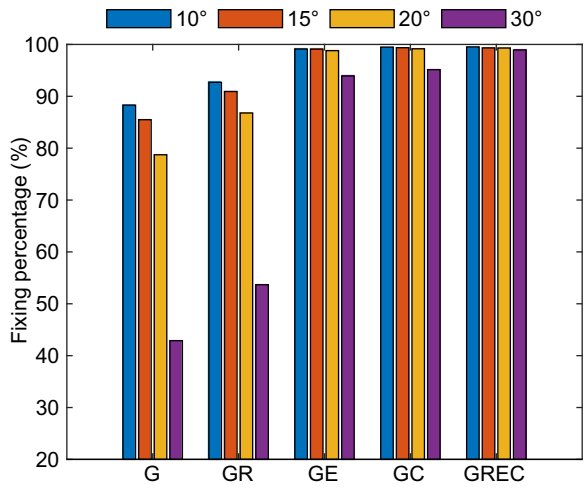

Fig. 4 Fixing percentage of PPP-RTK in different combination modes with different cut-off elevation angles from 10° to 30° at station at HKSC in Hong Kong, China (Li et al., 2021a)

PPP–RTK with multi-frequency observations

The most recently launched GNSS satellites (such as GPS Block-IIF, BDS, and Galileo) operate with three or more frequencies. Under the multi-frequency environment, multiple observation combinations can be constructed to speed up the integer ambiguity resolution. Geng and Bock (2013) firstly proposed a GPS Triple-Frequency (TF) PPP-AR method by formulating an Ambiguity-Fixed Ionosphere-Free (AFIF) combination. The simulated results indicate that the success rate of NL ambiguity resolution can be up to 99% within 65 s, while that of dual-frequency PPP-AR is only 64% within 150 s. Then Gu et al. (2015) implemented the BDS phase bias estimation and investigated its application in triple-frequency PPP-AR. Since fixing L1 ambiguities still faces some difficulties, only Extra-Wide-Lane (EWL) and WL ambiguities are fixed in their study. Li et al. (2019a) investigated a combined triple-frequency PPP-AR model with Galileo and BDS observations. The results show that BDS + Galileo triple-frequency PPP fixed solution significantly improves the positioning accuracy by 36.7% and 7.4% compared to the dual-frequency solutions in the horizontal and vertical components, respectively. Furthermore, the five-frequency PPP AR methods were proposed to fully use BDS-3 and Galileo multi-frequency signals, respectively (Li et al., 2020b, 2020c). Geng et al. (2020) proposed an approach to accelerate PPP ambiguity resolution using multi-constellation triple-frequency observations, where the raw ambiguities were mapped to EWL, WL, and NL ambiguities for integer ambiguity resolution. Consequently, the Time To First Fix (TTFF) of 48% NL ambiguities resolution can be shortened to 2.7 min with 20–21 visible satellites, in contrast to 5.2 min for dual-frequency PPP.

On this basis, potential improvements are expected for PPP–RTK with the utilization of multi-frequency observations. Hou et al. (2022) proposed a phase-only multi-frequency PPP-RTK model using BeiDou data, which extends the dual-frequency model to a multi-frequency one and prevents the negative effect of BDS-2 satellite-induced code bias. Li et al. (2022d) proposed a multi-frequency PPP–RTK method and investigated its performance in kinematic scenarios. Figure 5 shows the positioning series of PPP, as well as dual-frequency and multi-frequency PPP–RTK in urban environments. Obviously, the PPP–RTK remarkably improves

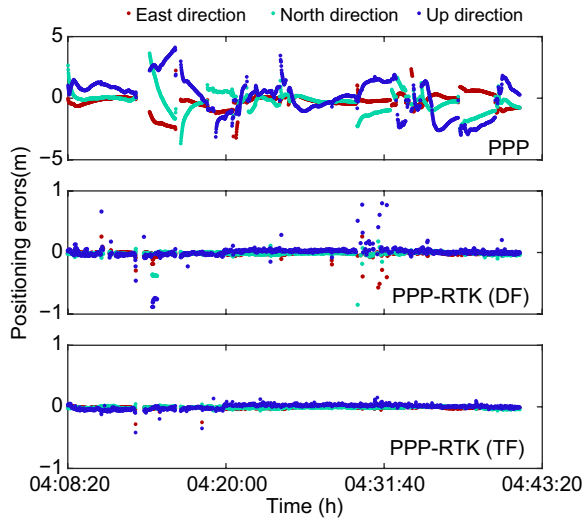

Fig. 5 Positioning series of PPP and dual-/tiple-frequency PPP-RTK in the urban environment. DF and TF indicate dual-frequency and triple-frequency, respectively

the performance of PPP in both convergence time and positioning accuracy. Compared to the dual-frequency solution, PPP–RTK with GPS, Galileo, and BDS multi-frequency observations presents a more precise and stable positioning series, particularly when the number of available satellites sharply decreases.

Low-cost PPP–RTK with single-frequency observations

With the increasing demand for precision location services, many scholars developed single-frequency PPP–RTK methods for low-cost applications. Odijk et al., (2012, 2014) firstly presented a CORS-based single-frequency PPP–RTK method based on the undifferenced model. The results showed that single-frequency PPP–RTK ambiguity resolution can be achieved within 2.5 min using a high-grade geodetic receiver and 5 min with a low-cost one. With the popularity of the multi-constellation GNSS, the single-frequency PPP–RTK models were extended to multi-GNSS combination. Then, Li et al. (2017c) proposed a new array-aided single-frequency PPP–RTK algorithm and validated it with L5/E5a observations of GPS, Galileo, IRNSS, and QZSS. Table 6 gives the RMSE in three directions and the average convergence time for single-frequency PPP–RTK solution. The results demonstrated that ambiguity resolution with centimeter-level accuracy can be achieved with combined multi-system single-frequency observations. Nadarajah et al. (2018) validated the performance of low-cost single-frequency PPP–RTK in small scales (with inter-station distances less than 30 km). In their experiments, single-frequency observations of three GNSS systems (GPS, Galileo and BDS) were used and the results showed that ambiguity can be fixed within 2 min.

Table 6 Empirical RMSE in North, East and Up components and average TTFF

Number of antennas in the array	RMSE (cm)			Average TTFF (s)
	N	E	U	
1	0.9	0.8	3.4	12
2	0.9	0.8	3.3	11
3	0.8	0.8	3.1	9
4	0.8	0.7	3.0	5

PPP–RTK for vehicle navigation

Due to the lack of real-time precise products, early PPP–RTK studies were usually conducted in a post-processing manner, and static data were used for the verification of positioning performance. With the improvement of various real-time precision products, PPP–RTK research has gradually shifted to real-time scenarios. Li et al. (2014) first validated the performance of the PPP–RTK method in a real-time scenario using the observations at the German SAPOS real-time stations and the real-time precise satellite products from the IGS real-time data analysis center at GFZ. The results indicate that the ambiguity can be fixed in one epoch for about 87% of the solution, and the RMS of the position errors is about 12, 10, and 25 mm in east, north, and up components, respectively. Afterward, the validation of multi-GNSS real-time PPP–RTK in different regions can be found in various studies (Li et al., 2020b, 2021c; Nadarajah et al., 2018).

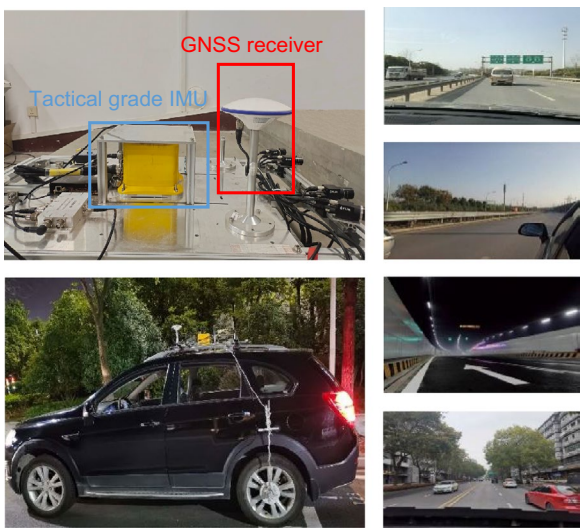

Fig. 6 Experimental equipment and typical scenes of vehicle test

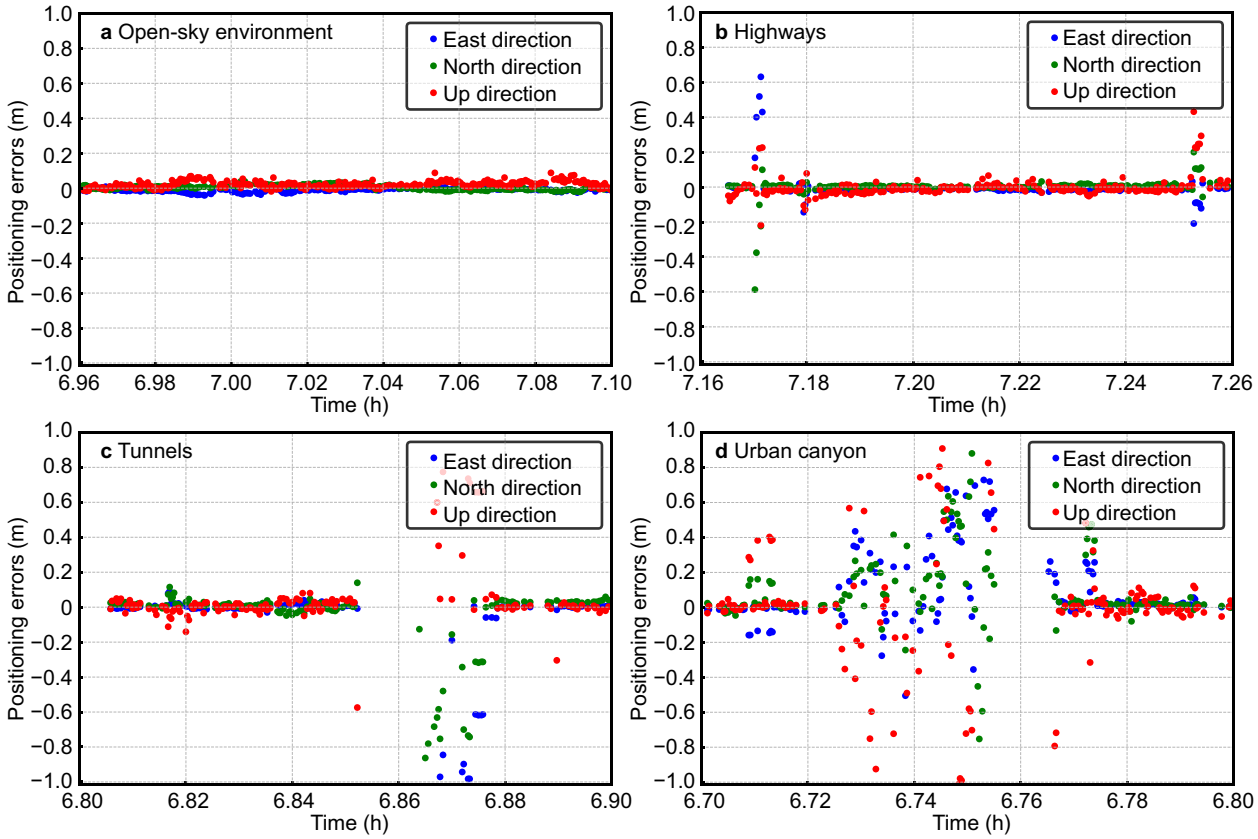

Fig. 7 Positioning error series of the PPP-RTK in different scenes

Recently, several vehicle experiments in typical urban scenes including suburbs, overpasses, and tunnels were conducted to validate the performance of the PPP–RTK method. Figure 6 shows the experimental equipment in vehicle tests including the hardware platform and the data acquisition device. At the same time, some typical experimental scenes are also shown in this figure. The tightly coupled RTK/INS solution solved by Inertial Explorer (IE) software typically provides the vehicle's reference trajectory.

The positioning series of the PPP–RTK in four different scenes are shown in Fig. 7. In an open-sky environment, PPP–RTK can obtain centimeter-level accuracy instantaneously and keep centimeter-accuracy solutions for a long period of time. When the vehicle runs on a highway, several re-convergence processes can be found because of the signal interruptions caused by obstructions such as overpasses or billboards. Fortunately, with the augmentation of atmospheric corrections, it takes just a few seconds for PPP–RTK solutions to re-converge to centimeter-level accuracy. Because of signal deterioration and blockage, PPP–RTK cannot work well in GNSS-challenged or denied environments such as tunnels or urban canyons where the positioning accuracy decreases to the meter level or more.

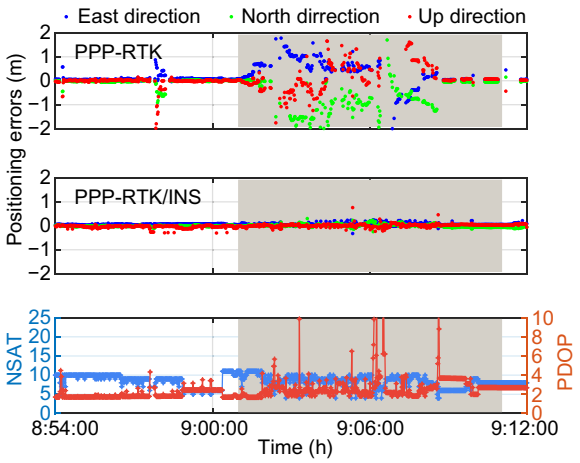

Fig. 8 Positioning series of PPP-RTK and tightly coupled PPP-RTK/INS in urban environments, respectively. The number of visible satellites (NSAT) and position dilution of precision (PDOP) series as well as the multipath series are also presented in the figure

In order to further improve the reliability and stability of PPP–RTK in complex urban environments, some scholars integrated PPP–RTK with other navigation and positioning techniques. Gu et al. (2021) and Li et al. (2021d) proposed PPP–RTK/Inertial Navigation System (INS) tightly coupled methods to enhance the positioning performance in urban areas. Two types of INS unit (a tactical inertial system and a MicroElectroMechanical System Inertial Measurement Units (MEMS-IMU)) were employed to verify the positioning performance. Figure 8 gives the positioning series of PPP–RTK and PPP–RTK/INS in an urban environment. It can be seen that the positioning performance of PPP–RTK can be significantly improved with the assistance of INS.

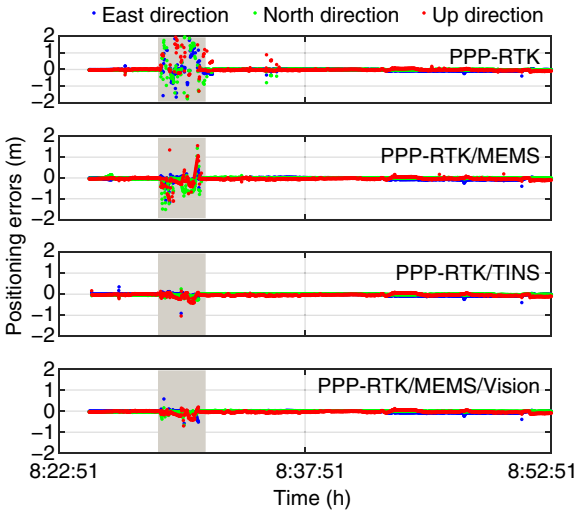

Fig. 9 Positioning series of PPP-RTK/MEMS, PPP-RTK/Tactical grade INS (PPP-RTK/TINS) and PPP-RTK/MEMS/vision

Li et al. (2022e) and Gu et al. (2022) further introduced visual sensor information to the PPP–RTK/INS system aiming to achieve continuous and accurate vehicle navigation in urban environments. Figure 9 shows the positioning series of PPP–RTK/MEMS, PPP–RTK/Tactical INS (PPP–RTK/TINS) and PPP–RTK /MEMS/vision, respectively. All the integrations are implemented in a tightly coupled model. One can see that the inclusion of vision information significantly improves the accuracy and reliability of PPP–RTK /MEMS and can achieve the comparable performance with the integration of PPP–RTK and tactical IMU.

Challenges and opportunities of PPP–RTK

Challenges

Several studies have been carried out on PPP–RTK focusing on the implementation method, performance analysis, and system applications. The results demonstrate the capability of PPP–RTK in providing rapid centimeter-accuracy positioning service. However, the performance of PPP–RTK faces challenges in some circumstances such as active ionosphere scenarios, complex terrain and weather conditions, and urban GNSS-challenge environments, which will be discussed in this section.

Ionospheric modeling in active ionosphere scenarios

The high-precision ionospheric modeling is significant to the performance of PPP–RTK. Previous research has shown that the slant ionospheric delay correction with

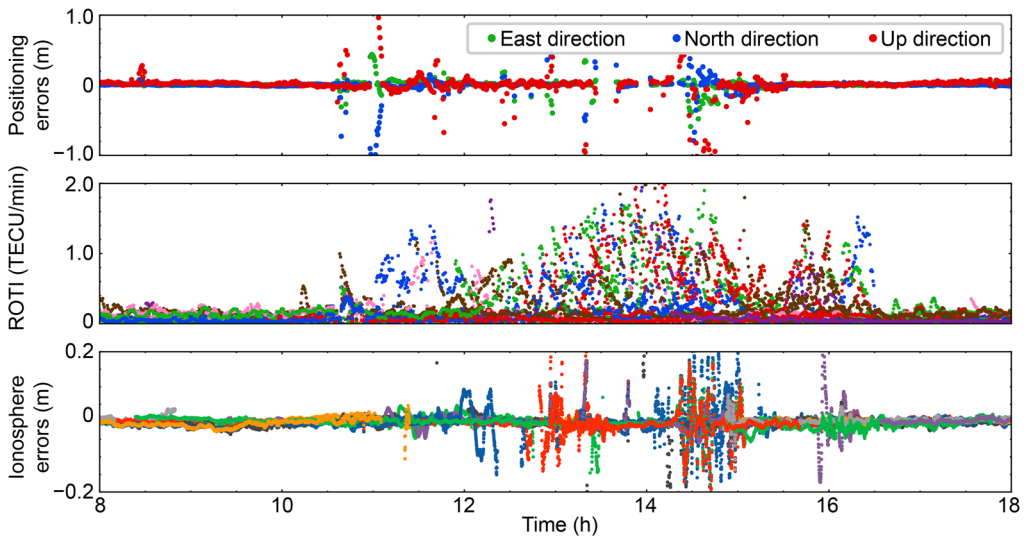

Fig. 10 Time series of PPP-RTK, ROTI, and interpolated ionosphere errors at HKSC station in Hong Kong, China

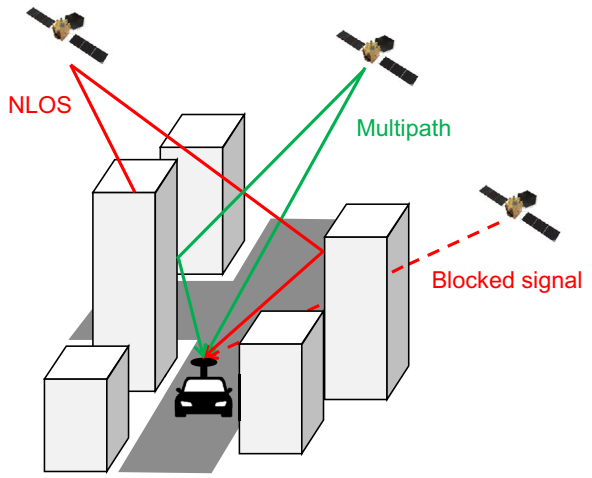

Fig. 11 Multipath, NLOS and blocked signals in city canyon

an accuracy of a few centimeters can be obtained by a regional network over a range of tens of kilometers. However, such an accuracy is unattainable in an active ionosphere scenario, such as a low-latitude region during the periods of high solar activity. Several investigations indicate that the ionospheric scintillation caused by ionospheric electron-density irregularities, has a negative impact on the precise positioning (Luo et al., 2018; Vilà-Valls et al. 2020). Figure 10 presents the time series of PPP–RTK, Rate Of Total Electron Content Index (ROTI), and ionospheric errors at a Hong Kong station HKSC. Here, the ionospheric error is calculated as the difference between the interpolated and extracted ionospheric delays at the user. ROTI is an important index referring to the occurrence of ionospheric scintillation. As can be seen, the performance of PPP–RTK is also greatly affected by the ionospheric scintillation during the period around 12:00 ~ 14:00 pm when the ROTI values are greatly increased, and the ionospheric errors exhibit obvious deviations. In this case, the PPP–RTK solution influenced by the ionospheric scintillation is unacceptable for some high-safety applications such as autonomous driving. Besides, Zhang et al. (2022) indicate that the high occurrence rate of Traveling Ionospheric Disturbance (TID, Hernández-Pajares et al., 2006, 2012) and its complicated characteristics also impact the operation of PPP–RTK service, especially at the beginning of each reinitialized period. Currently, the influence of ionosphere irregularities on PPP–RTK has been found, and more attention should be paid to the identification of ionosphere activities and the alleviation of its effect on the PPP–RTK.

Troposphere modeling under complex terrain and weather conditions

The signal propagation delay caused by the atmospheric water vapor is another important error affecting GNSS positioning performance, especially in terms of convergence time (Shi et al., 2014). There are two major challenges in modeling the tropospheric error in PPP–RTK. On the one hand, it is well known that the tropospheric error is highly related to the station position. Therefore, in the areas with complex terrain, a Two-Dimensional (2D) model that only considers the latitude and longitude is no longer applicable. A Three-Dimensional (3D) tropospheric model with high spatial resolution is highly required, especially in the areas with high altitude fluctuations. On the other hand, some extreme weather conditions cause the drastic changes in the troposphere. It will affect the tropospheric model's accuracy and, consequently, the positioning performance (Ma et al., 2021). Therefore, another challenge in troposphere modeling is how to identify the abnormal changes in the troposphere error and reflect the small-scale changes in the model. In the recent years, the accuracy and temporal-spatial resolution of meteorological data have been significantly improved (Lu et al., 2017), which makes a more accurate atmosphere model obtainable to enhance the performance of PPP–RTK by integrating the regional GNSS tropospheric delays with the meteorological products.

Signal occlusion and multipath

In urban environments, satellite signals are usually deteriorated or blocked due to the obstructions such as buildings, tall trees, overpasses, etc., which will degrade the performance of PPP–RTK. As shown in Fig. 11, we can see that the surrounding buildings block the view of satellites and their signals. The signals of these satellites finally arrive at the receiver but go through different reflections (None-Line-Of-Sight, NLOS) or multipath, thus causing large errors in the observations.

The multipath can be mitigated by hardware improvement and software processing. Since great efforts have been made in hardware level, which can efficiently eliminate partial multipath errors, most researchers recently focus on the data processing algorithm to further alleviate the multipath error, such as employing a filter to reduce the noise of time series and extract multipath (Han & Rizos, 1997), or proposing wavelet-based techniques to suppress the multipath-dominated frequency band (Su et al., 2018; Zhong et al., 2008). Zheng et al. (2019) compared the performance of the Sidereal Filtering (SF) model, Multipath Hemispherical Map (MHM) model, and a Modified Multipath Hemispherical Map

(M-MHM) model for mitigating the influence of multipath. The results show that the above models have a certain effect on reducing the multi-path error and improving the positioning accuracy. However, these methods utilize the spatiotemporal repeatability of the multipath in a static environment, which is not suitable for dynamic positioning. Recently, a wide field-of-view fish-eye camera mounted on the top of the vehicle was utilized to identify the NLOS satellites for the potential improvement in precise positioning (Sánchez et al. 2016; Wen et al. 2019). Besides, the well-known machine learning method has also been tried to solve the NLOS problems (Hsu, 2017; Suzuki and Amano, 2021). Consequently, some attempts for solving the problem of GNSS signal occlusion and multipath have been made, but further verifications are still needed for their applications in PPP–RTK.

Integrity monitoring

Integrity is a measure of the trustworthiness of the observations and products provided by the service system, which reflects the ability to correctly identify and eliminate the fault timely and to issue an alarm timely when the system is unavailable. The Integrity Monitoring (IM) methods of a navigation and positioning system can be divided into the IMs used in server-side and user-side. The server generates and broadcasts integrity information to all users. The most representative Satellite Autonomous Integrity Monitoring (SAIM) was originally proposed by Stanford University (Viearsson et al., 2001), whose essence is to install several onboard receivers on the satellite to integrate RAIM into the space segment. Extended to the inter-satellite link later, it can realize the IM of the global signal in space (Mc Graw and Murphy, 2001; Wang et al., 2015). For a Wide Area Precise Positioning System (WAPPS), real-time IM is realized by using correction data and monitoring station data, which can effectively monitor step and drift faults (Wang and Shen 2020c). Nowadays, the carrier phase is also utilized for IM, such as the IM system built by Trimble for the CenterPoint RTX Fast positioning service (Ulrich et al., 2018).

The integrity monitoring in the user-side is also a very important part in a navigation and positioning system. The concept of Receiver Autonomous Integrity Monitoring (RAIM) was proposed as early as 1987. The principle is to use the receiver's redundant observations for consistency check to detect and eliminate satellite faults. Initially, the IM algorithm used the pseudorange residual as the test quantity, mainly including the pseudorange comparison method (Lee, 1986), the least squares residual method (Parkinson & Axelrad, 1988), the parity vector method (Sturza, 1988) and the Kalman filter algorithm (Brown and Hwang, 1986) et al. After years of research, most of these methods have been improved to some extent (Susmita, 2016) and began to use the carrier phase for IM (Feng et al., 2009, 2012). At the same time, some new methods have emerged, such as the Solution Separation method (Pervan et al., 1998; Kazuma et al., 2019; Juan et al., 2020), the advanced RAIM (ARAIM, Juan et al., 2012; Phelts et al., 2020) et al. Compared with server-side IM, RAIM is easier to implement and has lower cost, which is currently a widely used IM method.

Recently, some achievements in IM have been made in the fields of high-precision GNSS applications such as vehicle navigation, autonomous driving, and aviation, etc. (Gianluca et al., 2010; Laura et al., 2019). However, for a PPP–RTK system, including real-time orbit and clock, UPD, and atmospheric corrections in the server as well as positioning solution at the user, the relevant research is still limited, and an efficient and reliable IM method is required (Garrett & Sunil, 2013; Altti et al., 2013; Merino and Laínez 2012; Navarro Madrid et al., 2015).

Opportunities

In recent years, the quality of multi-GNSS observations on smart devices has been gradually improved, rendering the high-precision positioning based on PPP–RTK accessible to mass users. In addition, the construction of Low Earth Orbit (LEO) constellations and the development of autonomous robotic navigation have given great opportunities for the development and application of PPP–RTK. The hotpots of new opportunities include the smart device-based applications, LEO augmentation, and multi-sensor fusion.

PPP–RTK on smart device

Currently, the Google Android allows access to acquire GNSS raw observations, making it possible to achieve high-precision positioning on low-cost devices by processing raw GNSS data with advanced and improved algorithms (Gao et al., 2021; Li & Geng, 2019; Odolinski & Teunissen, 2017; Zhang et al., 2018a). Nevertheless, because of the high noise level of raw observations from smart devices, only decimeter and sub-meter accuracy can be obtained (Psychas et al., 2019; Wu et al., 2019; Zhang et al., 2018b). PPP–RTK will make centimeter-accuracy and no-initialization positioning possible in low-cost smart devices, facilitating their pluralistic applications in the GNSS service market (Verhagen et al., 2010), such as a person or vehicle Location Based Service (LBS) and crowdsourced mapping. Since the positioning performance highly relies on the data quality, Li et al. (2022f) suggested to use an external antenna to further augment the positioning solutions. Figure 12 gives the equipment sets of GNSS smart device with low-cost

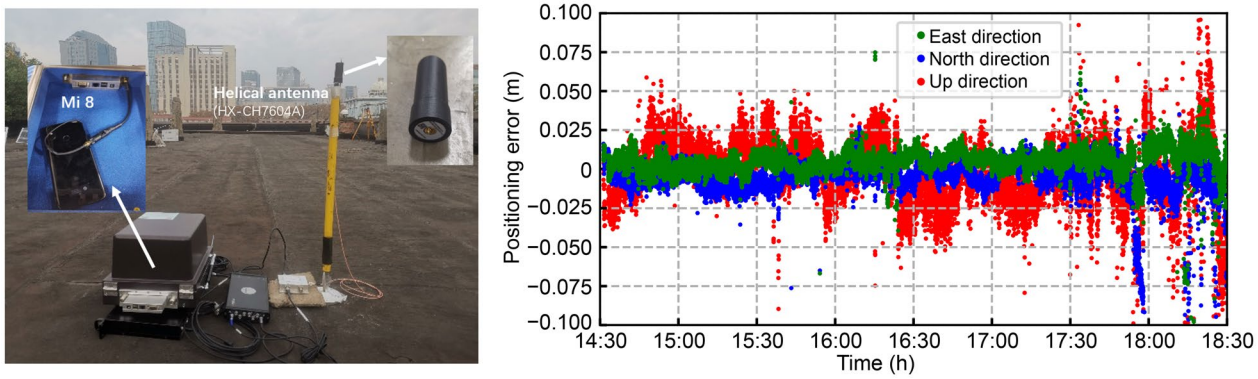

Fig. 12 Equipment sets of smart devices with the low-cost helical antenna (left panel) and PPP-RTK positioning series from 14:30 to 18:30 (right panel) (Li et al., 2022f)

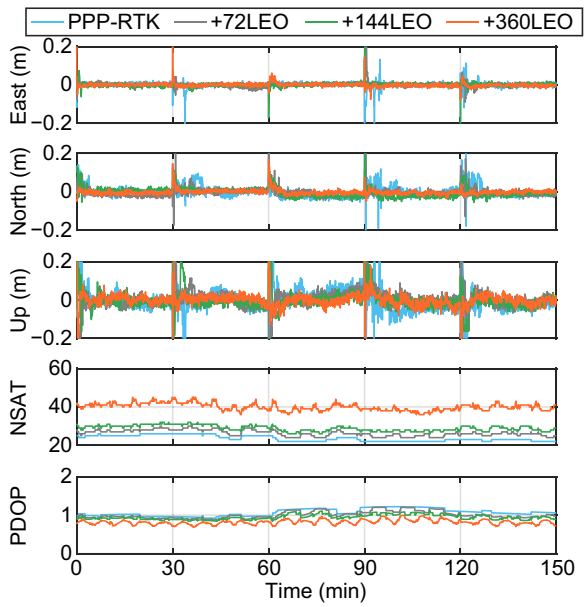

Fig. 13 Positioning series of PPP-RTK with the augmentation of different LEO constellations for an 800 km spaced network

helical antenna and presents the PPP–RTK positioning time series. The results show that the smartphone-based PPP–RTK can obtain centimeter-level positioning accuracy. This contribution gives a scheme that uses a smartphone and a low-cost antenna to achieve high-precision positioning, which has the potential to be widely used.

LEO augmented PPP–RTK

LEO satellites with an orbit altitude ranging from 300 to 1500 km, have several advantages such as strong signal strength and fast geometry change, which brings new opportunities for rapid precise positioning on a large scale. The results of the simulated experiments have shown that the convergence time of the float PPP can be shortened to several minutes with LEO augmentation (Ge et al., 2018, 2022; Li et al., 2019b, 2019c). Since the PPP–RTK relies on regional network augmentation to achieve rapid integer ambiguity resolution, it will face restrictions to the distribution and the inter-station distance of regional networks. It is expected that by introducing the LEO observations, PPP–RTK will be greatly enhanced, and a wide-area and high-precision positioning will be achieved. Figure 13 shows our simulated results of the positioning series of PPP–RTK with the augmentation of different LEO constellations for a large-scale network with an average spacing of 800 km. Three LEO constellations consisting of 72, 144, and 360 satellites are designed and used for the demonstration. As expected, the performance of PPP–RTK is improved significantly with the observations from the LEO constellation. A much faster initialization of a few seconds is obtained with the augmentation of LEO constellations. For a large-scale region with a spacing of 800 km, the average TTFF is reduced from 161 to 12 s with the augmentation of the 360-LEO constellation.

Since most LEO constellations are still under construction, the research on the demonstration of the LEO navigation system is generally based on simulated data. Once the actual LEO observations are employed, more issues for LEO-augmented PPP–RTK should be noted. For example, the LEO satellites are usually equipped with low-cost clocks, which makes it difficult to provide accurate clock products as GNSS satellites. In addition, because of the low altitude and the fast motion of the LEO satellites, the visible arc of a LEO satellite is about 10–15 min. Such a frequent alternation will result in more cycle clips, which has a negative impact on LEO data processing. In conclusion, LEO-augmented

PPP–RTK can effectively expand the scope of real-time precise positioning service and improve its positioning performance, but it also puts forward higher demands on the precise products and the advanced data processing approach of LEO satellites.

Multi-sensor augmented PPP–RTK

Nowadays, accurate and reliable positioning in full scenarios is of crucial importance for supporting emerging applications such as automatic cars and unmanned aerial vehicles. In an urban environment where GNSS signals are frequently blocked, a significant reduction in the availability and continuity of PPP–RTK positioning services can be found. INS can provide continuous navigation in a short period with no external information, making it as an effective supplement to GNSS in harsh satellite signal environments. In the past decades, PPP- and RTK-based GNSS/INS integrated algorithms were proposed, including Loose Coupling (LC) and Tight Coupling (TC), and demonstrated to significantly improve positioning accuracy and ambiguity fixing rate (Gao et al., 2017; Li et al., 2017b; Liu et al., 2016; Martell, 2009; Zhang et al., 2019). Recently, some researchers paid their attention to the integration of PPP–RTK and INS (Gu et al., 2021; Li et al., 2021d).

In addition, with the development of Simultaneous Localization and Mapping (SLAM), the fusion of cameras, LiDAR, and IMU are widely employed for navigation of autonomous devices in GNSS-challenged scenarios (Li & Mourikis, 2012; Weiss et al., 2012). Therefore, some studies introduced camera, LiDAR, and wheel odometer into GNSS/INS integrated systems to further enhance the positioning capability in GNSS harsh environments (Angelino et al., 2012; Cao et al., 2021; Gao et al., 2018; Li et al., 2019d, 2021d; Lynen et al., 2013; Mascaro et al., 2018; Reuper et al., 2018). Recently, as an optimal choice for navigation in automatic applications, the PPP–RTK integrated with multiple sensors has tremendous potential for massive market and is becoming a research hotspot.

To further augment the positioning performance of PPP–RTK, more efforts can be put in the utilization of more sensors. Several issues on combining multiple sensors for precise positioning should be addressed. First, the accurate calibration of spatial relationships and unification of temporal systems are the prerequisites for consistent fusion. Multiple sensors bring more complex spatial relationships, therefore, a comprehensive calibration model for accurate spatial relationships among multiple sensors needs to be solved. Moreover, there are still many significant differences in the operation characteristics for different sensors, such as measurement noise, sampling rate, temporal and spatial complexity of data processing, etc. It is challenging to check the reliability and accuracy of various types of measurement and to construct a stable and continuous positioning framework for integrated heterogeneous sensors.

Concluding remarks

Since the concept of PPP–RTK was proposed in 2005, many efforts have been made in the principal investigation and performance analysis of PPP–RTK. In recent years, with the rapid development of multi-GNSS and widely available real-time service, significant contributions are paid to multi-constellation and multi-frequency PPP–RTK, low-cost PPP–RTK, and its real-time vehicle navigation applications. Currently, the PPP–RTK technique with the capability to provide a centimeter-accuracy positioning service is regarded as a reliable tool for real-time positioning and navigation service and implemented in governmental and commercial systems. Nevertheless, there are still some potential challenges in PPP–RTK for a better performance, such as:

- How to obtain accurate ionospheric corrections in active ionosphere scenarios?
- How to develop a high-accuracy tropospheric model with high temporal and spatial resolution that adapts to complex terrain conditions and extreme weather events?
- How to mitigate the impact of signal occlusion and multipath on PPP–RTK processing in urban environments?

Meanwhile, the reduction of the cost of navigation components and the construction of massive LEO constellations give new possibilities for the development of PPP–RTK system and applications. Smart device, LEO augmentation, and multi-sensor fusion for PPP–RTK will be the research topics.

Acknowledgements

The algorithm results of PPP–RTK in this study is based on the GNSS+ REsearch, Application and Teaching (GREAT) software developed by the GREAT Group, School of Geodesy and Geomatics, Wuhan University.

Author contributions

XXL, X.L. and J.H. proposed the idea, processed the GNSS data, and wrote this paper. Z.S., JJ.H. L.L and B.W. assisted in paper writing and revision. All authors read and approved the final manuscript.

Funding

This work has been supported by National Science Fund for Distinguished Young Scholars (Grant No. 41825009), the National Postdoctoral Program for Innovative Talents, China (No. BX20220239), the Fundamental Research Funds for the Central Universities (2042022kf1001), and the Project Supported by the Special Fund of Hubei Luojia Laboratory (220100006).

Availability of data and materials

The datasets used and analyzed in this study are available from the corresponding author on reasonable request.

Declarations

Competing interests

The authors declare that they have no competing interests.

Author details

[1]School of Geodesy and Geomatics, Wuhan University, 129 Luoyu Road, Wuhan 430079, Hubei, China. [2]Technische Universitat Berlin (TUB), Straße Des 17. Juni, 10623 Berlin, Germany. [3]China Railway Siyuan Survey and Design Group Co., Ltd., Wuhan, China.

Received: 1 August 2022 Accepted: 15 November 2022
Published online: 06 December 2022

References

Al-Shaery, A., Lim, S., & Rizos, C. (2011). Investigation of different interpolation methods used in network-RTK for virtual reference station technique. *Journal of Global Positioning Systems, 10*(2), 136–148. https://doi.org/10.5081/jgps.10.2.136

Altti, J., Shaojun, F., Wolfgang, S., Washington, O., Chris, H., Terry, M., & Chris, H. (2013). Integrity monitoring of fixed ambiguity Precise Point Positioning (PPP) solutions. *Geo-Spatial Information Science, 16*(3), 141–148. https://doi.org/10.1080/10095020.2013.817111

Angelino V., Baraniello R., & Cicala L. (2012). UAV position and attitude estimation using IMU, GNSS and camera. In *2012 15th International Conference on Information Fusion*. Singapore (pp. 735–742).

Banville, S., Geng, J., Loyer, S., Schaer, S., Springer, T., & Strasser, S. (2020). On the interoperability of IGS products for precise point positioning with ambiguity resolution. *Journal of Geodesy, 94*(1), 10. https://doi.org/10.1007/s00190-019-01335-w

Bevis, M., Businger, S., Herring, A., Rocken, C., Anthes, A., & Ware, H. (1992). GPS meteorology: Remote sensing of atmospheric water vapor using the global positioning system. *Journal of Geophysical Research: Atmospheres, 97*(D14), 15787–15801.

Brown, G., & Hwang, P. (1986). GPS failure detection by autonomous means within the cockpit. *Navigation - Journal of the Institute of Navigation, 33*, 335–353.

Cabinet Office. (2020). *Quasi-Zenith Satellite System performance standard (PS-QZSS-002)*. https://qzss.go.jp/en/technical/download/pdf/ps-is-qzss/ps-qzss-002.pdf?t=1618040032826

Cao, S., Lu, X., & Shen, S. (2021). GVINS: Tightly coupled GNSS-visual-inertial for smooth and consistent state estimation. *IEEE Transactions on Robotics*. https://doi.org/10.1109/TRO.2021.3133730

Ciraolo, L., Azpilicueta, F., Brunini, C., Meza, A., & Radicella, M. (2007). Calibration errors on experimental slant total electron content (TEC) determined with GPS. *Journal of Geodesy, 81*, 111–120. https://doi.org/10.1007/s00190-006-0093-1

Collins, P. (2008). Isolating and estimating undifferenced GPS integer ambiguities. In *Proceedings of the 2008 national technical meeting of the institute of navigation*, San Diego, CA, USA (pp. 720–732).

Dai, L., Han, S., Wang, J., & Rizos, C. (2003). Comparison of interpolation algorithms in network-based GPS techniques. *Navigation - Journal of the Institute of Navigation, 50*(4), 277–293. https://doi.org/10.1002/j.2161-4296.2003.tb00335.x

Deng, Y., Guo, F., Ren, X., Ma, F., & Zhang, X. (2021). Estimation and analysis of multi-GNSS observable-specific code biases. *GPS Solutions, 25*(3), 1–13. https://doi.org/10.1007/s10291-021-01139-6

Dong, D., & Bock, Y. (1989). Global positioning system network analysis with phase ambiguity resolution applied to crustal deformation studies in California. *Journal of Geophysical Research, 94*(B4), 3949–3966.

Duan, J., Bevis, M., Fang, P., Bock, Y., Chiswell, S., Businger, S., Rocken, C., Solheim, F., van Hove, T., Ware, R., McClusky, S., & King, W. (1996). GPS meteorology: Direct estimation of the absolute value of precipitable water. *Journal of Applied Meteorology and Climatology, 35*(6), 830–838.

Feng, S., Washington, O., Terry, M., Chris, H., & Chris, H. (2009). Carrier phase-based integrity monitoring for high-accuracy positioning. *GPS Solutions, 13*, 13–22. https://doi.org/10.1007/s10291-008-0093-0

Feng, S., Ochieng, W., Samson, J., Tossaint, M., Hernandez-Pajares, M., Juan, J. M., Sanz, J., Aragón-Àngel, À., Ramos-Bosch, P., & Jofre, M. (2012). Integrity monitoring for carrier phase ambiguities. *Journal of Navigation, 65*(1), 41–58. https://doi.org/10.1017/S037346331100052X

Fotopoulos, G. (2000) Parameterization of carrier phase corrections based on a regional network of reference stations. In *Proceedings of the 13th international technical meeting of the satellite division of the institute of navigation (ION GPS 2000)*. Salt Lake City, UT, USA (pp. 1093–1102).

Gao Y., Li Z., & McLellan J. F. (1997). Carrier phase based regional area differential GPS for decimeter-level positioning and navigation. In *Proceedings of the 10th international technical meeting of the satellite division of the institute of navigation (ION GPS 1997)*. Kansas City, MO, USA (pp. 1305–1313).

Gao, Z., Zhang, H., Ge, M., Niu, X., Shen, W., Wickert, J., & Schuh, H. (2017). Tightly coupled integration of multi-GNSS PPP and MEMS inertial measurement unit data. *GPS Solutions, 21*(2), 377–391.

Gao, Z., Ge, M., Li, Y., Chen, Q., Zhang, Q., Niu, X., Zhang, H., Shen, W., & Harald, S. (2018). Odometer, low-cost inertial sensors, and four-GNSS data to enhance PPP and attitude determination. *GPS Solutions, 22*(3), 1–16.

Gao, R., Xu, L., Zhang, B., & Liu, T. (2021). Raw GNSS observations from Android smartphones: Characteristics and short-baseline RTK positioning performance. *Measurement Science and Technology, 32*, 8. https://doi.org/10.1088/1361-6501/abe56e

Garrett S., & Sunil B. (2013). Integrity monitoring in Precise Point Positioning. York University, Toronto, Canada. In *Proceedings of the 26th international technical meeting of the ION satellite division*, ION GNSS+2013. Nashville, TN, USA (pp. 1164–1175)

Ge, M., Gendt, G., Rothacher, M., Shi, C., & Liu, J. (2008). Resolution of GPS carrier-phase ambiguities in precise point positioning (PPP) with daily observations. *Journal of Geodesy, 82*(7), 389–399. https://doi.org/10.1007/s00190-007-0187-4

Ge, H., Li, B., Ge, M., Zang, N., Nie, L., Shen, Y., & Schuh, H. (2018). Initial assessment of precise point positioning with LEO enhanced global navigation satellite systems (LeGNSS). *Remote Sensing, 10*(7), 984.

Ge, H., Li, B., Jia, S., Nie, L., Wu, T., Yang, Z., Shang, J., Zheng, Y., & Ge, M. (2022). LEO enhanced global navigation satellite system (LeGNSS): Progress, opportunities, and challenges. *Geo-Spatial Information Science, 25*(1), 1–13.

Geng, J., & Bock, Y. (2013). Triple-frequency GPS precise point positioning with rapid ambiguity resolution. *Journal of Geodesy, 87*(5), 449–460.

Geng, J., & Bock, Y. (2016). GLONASS fractional-cycle bias estimation across inhomogeneous receivers for PPP ambiguity resolution. *Journal of Geodesy, 90*, 379–396. https://doi.org/10.1007/s00190-015-0879-0

Geng, J., Meng, X., Dodson, A. H., & Teferle, F. N. (2010). Integer ambiguity resolution in precise point positioning: Method comparison. *Journal of Geodesy, 84*, 569–581. https://doi.org/10.1007/s00190-010-0399-x

Geng, J., Teferle, F. N., Meng, X., & Dodson, A. H. (2011). Towards PPP–RTK: Ambiguity resolution in real-time precise point positioning. *Advances in Space Research, 47*(10), 1664–1673.

Geng, J., Guo, J., Meng, X., & Gao, K. (2020). Speeding up PPP ambiguity resolution using triple-frequency GPS/BDS/Galileo/QZSS data. *Journal of Geodesy, 94*, 1–15. https://doi.org/10.1007/s00190-019-01330-1

Gianluca G., Mauro L., Matteo Z., & Giancarlo V. (2010). GNSS integrity and protection level computation for vehicular applications. In *Proceedings of 16th Ka and broadband communications–navigation and earth observation conference*. Milan, Italy (pp. 569–574).

Gu, S., Lou, Y., Shi, C., & Liu, J. (2015). BeiDou phase bias estimation and its application in precise point positioning with triple-frequency observable. *Journal of Geodesy, 89*(10), 979–992.

Gu, S., Dai, C., Fang, W., Zheng, F., Wang, Y., Zhang, Q., Lou, Y., & Niu, X. (2021). Multi-GNSS PPP/INS tightly coupled integration with atmospheric augmentation and its application in urban vehicle navigation. *Journal of Geodesy, 95*, 1–15. https://doi.org/10.1007/s00190-021-01514-8

Gu, S., Dai, C., Mao, F., & Fang, W. (2022). Integration of multi-GNSS PPP–RTK / INS/Vision with a cascading Kalman filter for vehicle navigation in urban areas. *Remote Sensing, 14*, 4337. https://doi.org/10.3390/rs14174337

Han, S. (1997). *Carrier phase-based long-range GPS kinematic positioning*. Ph.D. Dissertation, School of Geomatic Engineering, The University of New South Wales, Sydney, Australia.

Han S., & Rizos C. (1997). Multipath effects on GPS in mine environments. In *10th international congress of the International Society for Mine Surveying Fremantle*, Australia.

Hernández-Pajares, M., Juan, J. M., & Sanz, J. (2006). Medium-scale traveling ionospheric disturbances affecting GPS measurements: Spatial and temporal analysis. *Journal of Geophysical Research Atmospheres*, *111* (A7), A07S11. https://doi.org/10.1029/2005JA011474.

Hernández-Pajares, M., Juan, J. M., Sanz, J., & Aragón-Àngel, A. (2012). Propagation of medium scale traveling ionospheric disturbances at different latitudes and solar cycle conditions. *Radio Science, 47*, 1–22. https://doi.org/10.1029/2011RS004951

Hofmann-Wellenhof, B., Lichtenegger, H., & Collins, J. (2001). *Global positioning system: Theory and practice*. Springer.

Hopfield, H. S. (1972). *Tropospheric range error parameters: Further studies 46*. https://doi.org/NASA-CR-127559, APL/JHU-CP-015

Hou, P., Zhang, B., Yasyukevich, Y. V., Liu, T., & Zha, J. (2022). Multi-frequency phase-only PPP–RTK model applied to BeiDou data. *GPS Solutions, 26*, 76. https://doi.org/10.1007/s10291-022-01263-x

Hsu, L. T. (2017). GNSS multipath detection using a machine learning approach. In *IEEE international conference on intelligent transportation systems*. Yokohama, Japan (pp. 1–6). https://doi.org/10.1109/ITSC.2017.8317700

Hu, J., Zhang, X., Li, P., Ma, F., & Pan, L. (2020). Multi-GNSS fractional cycle bias products generation for GNSS ambiguity-fixed PPP at Wuhan University. *GPS Solutions, 24*(1), 15.

Juan, B., Todd, W., & Per, E. (2012). Advanced RAIM user algorithm description: Integrity support message processing, fault detection, exclusion, and protection level calculation. In *Proceedings of the 25th international technical meeting of the satellite division of the Institute of Navigation (ION GNSS 2012)*. Nashville, TN, USA (pp. 2828–2849).

Juan, B., Todd, W., Laura, N., Kazuma, G., & Lance, G. (2020). Solution separation-based FD to mitigate the Effects of Local Threats on PPP Integrity. In *2020 IEEE/ION Position, Location and Navigation Symposium (PLANS)*. Portland, OR, USA (pp. 1085–1092).

Kazuma, G., Juan, B., & Todd, W. (2019). SBAS corrections for PPP integrity with solution separation. In *Proceedings of the 2019 international technical meeting of the Institute of Navigation*. Reston, Virginia, USA (pp. 707–719). https://doi.org/10.33012/2019.16739

Khodabandeh, A., & Teunissen, P. J. G. (2016). PPP–RTK and inter-system biases: The ISB look-up table as a means to support multi-system PPP–RTK. *Journal of Geodesy, 90*, 837–851.

Khodabandeh, A., & Teunissen, P. J. G. (2018). On the impact of GNSS ambiguity resolution: Geometry, ionosphere, time and biases. *Journal of Geodesy, 92*(6), 637–658.

Laura, N., Eduardo, I., & de Groot, L. (2019). Integrity performance for precise positioning in automotive. In *32nd international technical meeting of the satellite division of the Institute of Navigation (ION GNSS+ 2019)*Miami, Florida, USA (pp. 1653–1663).

Laurichesse, D., & Mercier, F. (2007). Integer ambiguity resolution on undifferenced GPS phase measurements and its application to PPP. In *20th international technical meeting of the satellite division of the Institute of Navigation (2007 ION GNSS)*. Fort Worth, TX, USA (pp. 839–848).

Laurichesse, D., Mercier, F., Berthias, J. P., Broca, P., & Cerri, L. (2009). Integer ambiguity resolution on undifferenced GPS phase measurements and its application to PPP and satellite precise orbit determination. *Navigation - Journal of the Institute of Navigation, 56*(2), 135–149. https://doi.org/10.1002/j.2161-4296.2009.tb01750.x

Lee, Y. (1986). Analysis of range and position comparison methods as a means to provide GPS integrity in the user receiver. In *Institute of navigation 42nd annual meeting*. Seattle, Washington, USA (pp. 1–4).

Li, M., & Mourikis, A. I. (2012). Improving the accuracy of EKF-based visual-inertial odometry. In *Proceedings of the IEEE international conference on robotics and automation*. Saint Paul, MN, USA (pp. 828–835).

Li, X., & Zhang, X. (2012). Improving the estimation of uncalibrated fractional phase of sets for PPP ambiguity resolution. *Navigation - Journal of the Institute of Navigation, 65*(3), 513–529.

Li, G., & Geng, J. (2019). Characteristics of raw multi-GNSS measurement error from Google Android smart devices. *GPS Solutions, 23*, 1–16.

Li, X., Zhang, X., & Ge, M. (2011). Regional reference network augmented precise point positioning for instantaneous ambiguity resolution. *Journal of Geodesy, 85*(3), 151–158. https://doi.org/10.1007/s00190-010-0424-0

Li, X., Ge, M., Zhang, H., & Wickert, J. (2013). A method for improving uncalibrated phase delay estimation and ambiguity-fixing in real-time precise point positioning. *Journal of Geodesy, 87*, 405–416. https://doi.org/10.1007/s00190-013-0611-x

Li, X., Dick, G., Ge, M., Helse, S., Wickert, J., & Bender, M. (2014). Real-time GPS sensing of atmospheric water vapor: Precise point positioning with orbit, clock, and phase delay corrections. *Geophysical Research Letters, 41*, 3615–3621. https://doi.org/10.1002/2013GL058721

Li, X., Ge, M., Dai, X., Ren, X., Fritsche, M., Wickert, J., & Schuh, H. (2015). Accuracy and reliability of multi-GNSS real-time precise positioning: GPS, GLONASS, BeiDou, and Galileo. *Journal of Geodesy, 89*, 607–635. https://doi.org/10.1007/s00190-015-0802-8

Li, P., Zhang, X., & Guo, F. (2017a). Ambiguity resolved precise point positioning with GPS and BeiDou. *Journal of Geodesy, 91*(1), 25–40.

Li, T., Zhang, H., Niu, X., & Gao, Z. (2017b). Tightly-coupled integration of multi-GNSS single-frequency RTK and MEMS-IMU for enhanced positioning performance. *Sensors, 17*(11), 2462–2484. https://doi.org/10.3390/s17112462

Li, W., Nadarajah, N., Teunissen, P. J. G., & Khodabandeh, A. (2017c). Array-aided single-frequency state-space RTK with combined GPS, Galileo, IRNSS, and QZSS L5/E5a observations. *Journal of Surveying Engineering, 143*(4), 04017006.

Li, X., Li, X., Yuan, Y., Zhang, K., Zhang, X., & Wickert, J. (2018). Multi-GNSS phase delay estimation and PPP ambiguity resolution: GPS, BDS, GLONASS, Galileo. *Journal of Geodesy, B4*, 1–30. https://doi.org/10.1007/s00190-017-1081-3

Li, X., Liu, G., Feng, G., Yuan, Y., Zhang, K., & Ren, X. (2019a). Triple-frequency PPP ambiguity resolution with multi-constellation GNSS: BDS and Galileo. *Journal of Geodesy, 93*(8), 1105–1122.

Li, X., Ma, F., Li, X., Lv, H., Bian, L., Jiang, Z., & Zhang, X. (2019b). LEO Constellation-augmented multi-GNSS for Rapid PPP Convergence. *Journal of Geodesy, 93*(5), 749–764. https://doi.org/10.1007/s00190-018-1195-2

Li, B., Ge, H., Ge, M., Nie, L., Shen, Y., & Schuh, H. (2019c). LEO enhanced global navigation satellite system (Legnss) for real-time precise positioning services. *Advances in Space Research, 63*(1), 73–93. https://doi.org/10.1016/j.asr.2018.08.017

Li, T., Zhang, H., Gao, Z., Niu, X., & El-Sheimy, N. (2019d). Tight fusion of a monocular camera, MEMS-IMU, and single-frequency multi-GNSS RTK for precise navigation in GNSS-Challenged environments. *Remote Sensing, 11*(6), 610.

Li, Z., Chen, W., Ruan, R., & Liu, X. (2020a). Evaluation of PPP–RTK based on BDS-3/BDS-2/GPS observations: A case study in Europe. *GPS Solutions, 24*(2), 1–12.

Li, X., Liu, G., Li, X., Zhou, F., Feng, G., Yuan, Y., & Zhang, K. (2020b). Galileo PPP rapid ambiguity resolution with five-frequency observations. *GPS Solutions, 24*(1), 1–13. https://doi.org/10.1007/s10291-019-0930-3

Li, X., Li, X., Liu, G., Yuan, Y., Freeshah, M., Zhang, K., & Zhou, F. (2020c). BDS multi-frequency PPP ambiguity resolution with new B2a/B2b/B2a + b signals and legacy B1I/B3I signals. *Journal of Geodesy, 94*(100), 1–15. https://doi.org/10.1007/s00190-020-01439-8

Li, X., Huang, J., Li, X., Lyu, H., Wang, B., Xiong, Y., & Xie, W. (2021a). Multi-constellation GNSS PPP instantaneous ambiguity resolution with precise atmospheric corrections augmentation. *GPS Solutions, 25*(3), 1–13.

Li, X., Han, X., Li, X., Liu, G., Feng, G., Wang, B., & Zheng, H. (2021b). GREAT-UPD: An open-source software for uncalibrated phase delay estimation based on multi-GNSS and multi-frequency observations. *GPS Solutions, 25*(2), 1–9. https://doi.org/10.1007/s10291-020-01070-2

Li, X., Wang, X., Liao, J., Li, X., & Lyu, H. (2021c). Semi-tightly coupled integration of multi-GNSS PPP and S-VINS for precise positioning in GNSS-challenged environments. *Satellite Navigation, 2*(1), 1–14.

Li, X., Li, X., Huang, J., Shen, Z., Wang, B., Yuan, Y., & Zhang, K. (2021d). Improving PPP–RTK in urban environment by tightly coupled integration of GNSS and INS. *Journal of Geodesy, 95*(12), 1–18.

Li, B., Ge, H., Bu, Y., Zhang, Y., & Yuan, L. (2022a). Comprehensive assessment of real-time precise products from IGS analysis centers. *Satellite Navigation, 3*, 1–17. https://doi.org/10.1186/s43020-022-00074-2

Li, X., Li, X., Jiang, Z., Xia, C., Shen, Z., & Wu, J. (2022b). A unified model of GNSS phase/code bias calibration for PPP ambiguity resolution with GPS, BDS, Galileo and GLONASS multi-frequency observations. *GPS Solutions, 26*, 1–16. https://doi.org/10.1007/s10291-022-01269-5

Li, P., Cui, B., Hu, J., Liu, X., Zhang, X., Ge, M., & Schuh, H. (2022c). PPP–RTK considering the ionosphere uncertainty with cross-validation. *Satellite Navigation, 3*(1), 1–13. https://doi.org/10.1186/s43020-022-00071-5

Li, X., Wang, B., Li, X., Huang, J., Lyu, H., & Han, X. (2022d). Principle and performance of multi-frequency and multi-GNSS PPP–RTK. *Satellite Navigation, 3*(1), 1–11. https://doi.org/10.1186/s43020-022-00068-0

Li, X., Li, X., Li, S., Zhou, Y., Sun, M., Xu, Q., & Xu, Z. (2022e). Centimeter-accurate vehicle navigation in urban environments with a tightly integrated PPP–RTK /MEMS/vision system. *GPS Solutions, 26*, 124. https://doi.org/10.1007/s10291-022-01306-3

Li, X., Wang, H., Li, X., Li, L., Lv, H., Shen, Z., Xia, C., & Gou, H. (2022f). PPP rapid ambiguity resolution using Android GNSS raw measurements with a low-cost helical antenna. *Journal of Geodesy, 96*, 1–14. https://doi.org/10.1007/s00190-022-01661-6

Liu, S., Sun, F., Zhang, L., Li, W., & Zhu, X. (2016). Tight integration of ambiguity-fixed PPP and INS: Model description and initial results. *GPS Solutions, 20*(1), 39–49.

Liu, Y., Ye, S., Song, W., Lou, Y., & Chen, D. (2017a). Integrating GPS and BDS to shorten the initialization time for ambiguity-fixed PPP. *GPS Solutions, 21*(2), 333–343.

Liu, Y., Song, W., Lou, Y., Ye, S., & Zhang, R. (2017b). GLONASS phase bias estimation and its PPP ambiguity resolution using homogeneous receivers. *GPS Solutions, 21*(2), 427–437.

Liu, Y., Ye, S., Song, W., Lou, Y., & Gu, S. (2017c). Rapid PPP ambiguity resolution using GPS+GLONASS observations. *Journal of Geodesy, 91*(4), 441–455.

Lu, C., Li, X., Zus, F., Heinkelmann, R., Dick, G., Ge, M., Wickert, J., & Schuh, H. (2017). Improving BeiDou real-time precise point positioning with numerical weather models. *Journal of Geodesy, 91*(9), 1019–1029. https://doi.org/10.1007/s00190-017-1005-2

Luo, X., Lou, Y., Xiao, Q., Gu, S., Chen, B., & Liu, Z. (2018). Investigation of ionospheric scintillation effects on BDS precise point positioning at low-latitude regions. *GPS Solutions, 22*(63), 1–12. https://doi.org/10.1007/s10291-018-0728-8

Lynen, S., Achtelik, M. W., Weiss, S., Chli, M., & Siegwart, R. (2013). A robust and modular multi-sensor fusion approach applied to MAV navigation. In *IEEE/RSJ international conference on intelligent robots and systems*. Tokyo, Japan (pp. 3923–3929).

Ma, H., Zhao, Q., Verhagen, S., Psychas, D., & Liu, X. (2020). Assessing the performance of multi-GNSS PPP–RTK in the local area. *Remote Sensing, 12*, 3343. https://doi.org/10.3390/rs12203343

Ma, H., Psychas, D., Xing, X., Zhao, Q., & Liu, X. (2021). Influence of the inhomogenous troposphere on gnss positioning and integer ambiguity resolution. *Advances in Space Research, 67*(2), 1914–1928.

Martell, H. (2009). Tightly coupled processing of precise point position (PPP) and ins data. In *Proceedings of the 22nd international technical meeting of the satellite division of the institute of navigation (ION GNSS 2009)*. Savannah, GA, USA (pp. 1898–1905).

Mascaro, R., Teixeira, L., Hinzmann, T., Siegwart, R, & Chli, M. (2018). GOMSF: Graph-optimization based multi-sensor fusion for robust UAV pose estimation. In *IEEE international conference on robotics and automation (ICRA)*. Brisbane, QLD, Australia (pp. 1421–1428).

Mc Graw, G., & Murphy, T. (2001). Safety of life considerations for GPS modernization architectures. In *Proceedings of the 14th international technical meeting of the satellite division of the Institute of Navigation (ION GPS 2001)*. Salt Lake City, UT, USA (pp. 632–640).

Merino, M. M. R., Laínez, M. D. (2012). Integrity for advanced precise positioning applications. In *proceedings of the 25th International Technical Meeting of the Satellite Division of The Institute of Navigation (ION GNSS 2012). Nashville, TN, USA*. (pp. 2742–2758).

Montenbruck, O., Steigenberger, P., Khachikyan, R., Weber, G., Langley, R. B., Mervart, L., & Hugentobler, U. (2014). IGS-MGEX: Preparing the ground for multi-constellation GNSS science. *Inside GNSS, 9*(1), 42–49.

Montenbruck, O., Steigenberger, P., Prange, L., Deng, Z., Zhao, Q., Perosanz, F., Romero, I., Noll, C., Stürze, A., Weber, G., Schmid, R., Macleod, K., & Schaer, S. (2017). The multi-GNSS experiment (MGEX) of the international GNSS service (IGS)—Achievements, prospects and challenges. *Advances in Space Research, 59*, 1671–1697. https://doi.org/10.1016/j.asr.2017.01.011

Nadarajah, N., Khodabandeh, A., Wang, K., Choudhury, M., & Teunissen, P. J. G. (2018). Multi-GNSS PPP–RTK: From large- to small-scale networks. *Sensors, 18*(4), 1078. https://doi.org/10.3390/s18041078

Navarro Madrid, P. F., Laínez Samper, M. D., & Romay Merino, M. M. (2015). New approach for integrity bounds computation applied to advanced precise positioning applications. In *Proceedings of the 28th International technical meeting of the satellite division of the Institute of Navigation (ION GNSS+ 2015)*. Tampa, Florida, USA (pp. 2821–2834).

Odijk, D., Teunissen, P. J. G., & Zhang, B. (2012). Single-frequency integer ambiguity resolution enabled GPS precise point positioning. *Journal of Surveying Engineering, 138*(4), 193–202.

Odijk, D., Teunissen, P. J. G., & Khodabandeh, A. (2014). Single-frequency PPP–RTK: Theory and experimental results. *Earth on the edge: Science for a sustainable planet* (pp. 571–578). Berlin: Springer.

Odijk, D., Zhang, B., Khodabandeh, A., Odolinski, R., & Teunissen, P. J. G. (2016). On the estimability of parameters in undifferenced, uncombined GNSS network and PPP–RTK user models by means of S-system theory. *Journal of Geodesy, 90*, 15–44. https://doi.org/10.1007/s00190-015-0854-9

Odolinski, R., & Teunissen, P. J. G. (2017). On the performance of a low-cost single-frequency GPS+BDS RTK positioning model. In *Proceedings of the 2017 international technical meeting of the institute of navigation*. Monterey, California, USA (pp. 745–753).

Oliveira, P. S., Morel, L., Fund, F., Legros, R., Monico, J. F. G., Durand, S., & Durand, F. (2017). Modeling tropospheric wet delays with dense and sparse network configurations for PPP–RTK. *GPS Solutions, 21*, 237–250. https://doi.org/10.1007/s10291-016-0518-0

Parkinson, B., & Axelrad, P. (1988). Autonomous GPS integrity monitoring using the pseudorange residual. *Navigation - Journal of the Institute of Navigation 35*, 255–274.

Pervan, B., Pullen, S., & Christie, J. (1998). A multiple hypothesis approach to satellite navigation integrity. *Journal of Navigation., 45*(1), 61–71.

Phelts, R. E., Gunning, K., Blanch, J., & Walter, T. (2020). Evaluating the application of PPP techniques to ARAIM using flight data. In *Proceedings of the 2020 international technical meeting of the Institute of Navigation*. San Diego, California, USA (pp. 379–385). https://doi.org/10.33012/2020.17151

Psychas, D., & Verhagen, S. (2020). Real-time PPP-RTK performance analysis using ionospheric corrections from multi-scale network configurations. *Sensors, 20*(11), 3012. https://doi.org/10.3390/s20113012

Psychas, D., Bruno, J., Massarweh, L., & Darugna, F. (2019). Towards sub-meter positioning using android raw GNSS measurements. In *Proceedings of the 32nd international technical meeting of the satellite division of the institute of navigation (ION GNSS+ 2019)*. Miami, Florida, USA (pp. 3917–3931).

Psychas, D., Teunissen, P. J. G., & Verhagen, S. (2021). A multi-frequency Galileo PPP–RTK convergence analysis with an emphasis on the role of frequency spacing. *Remote Sensing, 13*, 3077. https://doi.org/10.3390/rs13163077

Raquet, J. F. (1997). Multiple user network carrier-phase ambiguity resolution. In *International symposium on kinematic systems in geodesy, geomatics & navigation (KIS1997)* (pp. 45–55).

Ren, X., Chen, J., Li, X., & Zhang, X. (2020). Ionospheric total electron content estimation using GNSS carrier phase observations based on zero-difference integer ambiguity: Methodology and assessment. *IEEE Transactions on Geoscience and Remote Sensing, 99*, 1–14. https://doi.org/10.1109/TGRS.2020.2989131

Reuper, B., Becker, M., & Leinen, S. (2018). Benefits of multi-constellation/multi-frequency GNSS in a tightly coupled GNSS/IMU/odometry integration algorithm. *Sensors, 18*(9), 3052.

Rizos, C. (2002). Network RTK research and implementation—A geodetic perspective. *Journal of Global Positioning Systems, 1*(2), 144–150. https://doi.org/10.5081/jgps.1.2.144

Rizos, C., Montenbruck, O., Weber, R., Neilan, R., & Hugentobler, U. (2013). The IGS MGEX experiment as a milestone for a comprehensive multi-GNSS service. In *Proceedings of the ION 2013 pacific PNT meeting (ION PNT 2013)*. Honolulu, Hawaii, USA (pp. 289–295).

Rovira-Garcia, A., Timoté, C. C., Juan, J. M., Sanz, J., González-Casado, G., Fernández-Hernández, I., Orus-Perez, R., & Blonski, D. (2021). Ionospheric corrections tailored to the Galileo High Accuracy Service. *Journal of Geodesy, 95*, 130. https://doi.org/10.1007/s00190-021-01581-x

Sánchez, J. S., Gerhmann, A., Thevenon, P., Brocard, P., Afia, A. B., & Julien, O. (2016). Use of a FishEye camera for GNSS NLOS exclusion and characterization in urban environments. In *Proceedings of the 2016 international*

technical meeting of the institute of navigation. Monterey, California, USA (pp. 283–292).
Shi, J., Xu, C., Guo, J., & Gao, Y. (2014). Local troposphere augmentation for real-time precise point positioning. *Earth, Planets and Space, 66*(1), 1–13. https://doi.org/10.1186/1880-5981-66-30
Sturza, M. (1988). Navigation system integrity monitoring using redundant measurements. *Journal of the Institute of Navigation, 35*(4), 483–501.
Su, M., Zheng, J., Yang, Y., & Wu, Q. (2018). A new multipath mitigation method based on adaptive thresholding wavelet denoising and double reference shift strategy. *GPS Solutions, 22*(2), 1–12. https://doi.org/10.1007/s10291-018-0708-z
Susmita, B. (2016). Kalman filter-based GNSS integrity monitoring. In *9th international technical meeting of the satellite division of the institute of navigation (ION GNSS+ 2016)*. Portland, Oregon, USA (pp. 1736–1749).
Suzuki, T., & Amano, Y. (2021). NLOS multipath classification of GNSS signal correlation output using machine learning. *Sensors, 21*(7), 2503. https://doi.org/10.3390/s21072503
Teunissen, P. J. G. (1995). The least squares ambiguity decorrelation adjustment: A method for fast GPS integer estimation. *Journal of Geodesy, 70*, 65–82.
Teunissen, P. J. G. (1998). Success probability of integer GPS ambiguity rounding and bootstrapping. *Journal of Geodesy, 72*(10), 606–612.
Teunissen, P. J. G. (1999). An optimality property of the integer leastsquares estimator. *Journal of Geodesy, 73*, 587–593.
Teunissen, P. J. G. (2019). A new GLONASS FDMA model. *GPS Solutions, 23*(4), 1–19. https://doi.org/10.1007/s10291-019-0889-0
Teunissen, P. J. G., & Khodabandeh, A. (2015). Review and principles of PPP-RTK methods. *Journal of Geodesy, 89*(3), 217–240.
Teunissen, P. J. G., Odijk, D., & Zhang, B. (2010). PPP-RTK: Results of CORS network-based PPP with integer ambiguity resolution. *Journal of Aeronautics, Astronautics and Aviation, Series A, 42*(4), 223–230.
Ulrich, W., Markus, B., Chen, X., Landau, H., Pastor, F., Reussner, N., & Rodriguez-Solano, C. (2018). Integrity of the Trimble CenterPoint RTX Correction Service. In *31st international technical meeting of the satellite division of the institute of navigation (ION GNSS+ 2018)*. Miami, Florida, USA (pp. 1902-1909).
Verhagen, S., Odijk, D., Teunissen, P., & Huisman, L. (2010). Performance improvement with low-cost multi-GNSS receivers. In *2010 5th ESA workshop on satellite navigation technologies and European workshop on GNSS signals and signal processing (NAVITEC)*. Noordwijk, Netherlands (pp. 1–8).
Viearsson, L., Pullen, S., Green, G., & Enge, P. (2001). Satellite autonomous integrity monitoring and its role in enhancing GPS user performance. In *Proceedings of the 14th international technical meeting of the satellite division of the institute of navigation (ION GPS 2001)*. Salt Lake City, Utah, USA (pp. 11–14).
Vilà-Valls, J., Linty, N., Closas, P., Dovis, F., & Curran, J. T. (2020). Survey on signal processing for GNSS under ionospheric scintillation: Detection, monitoring, and mitigation. *Navigation - Journal of the Institute of Navigation, 67*(3), 511–536.
Villiger, A., Schaer, S., Dach, R., Prange, L., Sušnik, A., & Jäggi, A. (2019). Determination of GNSS pseudo-absolute code biases and their long-term combination. *Journal of Geodesy, 93*(9), 1487–1500.
Wang, Y., & Shen, J. (2020). Real-time integrity monitoring for a wide area precise positioning system. *Satellite Navigation, 1*(1), 1–10. https://doi.org/10.1186/s43020-020-00018-8
Wang, Y., Li, R., & Zhao, R. (2015). Research of signal-in-space integrity monitoring based on inter-satellite links. *Chinese Journal of Electronics, 24*(2), 439.
Wang, N., Li, Z., Duan, B., Hugentobler, U., & Wang, L. (2020a). GPS and GLONASS observable-specific code bias estimation: Comparison of solutions from the IGS and MGEX networks. *Journal of Geodesy, 94*(8), 1–15.
Wang, S., Li, B., Gao, Y., Gao, Y., & Guo, H. (2020b). A comprehensive assessment of interpolation methods for regional augmented PPP using reference networks with different scales and terrains. *Measurement, 150*, 107067. https://doi.org/10.1016/j.measurement.2019.107067
Wanninger, L. (1995). Improved AR by regional differential modeling of the ionosphere. In *Proceedings of the 8th international technical meeting of the satellite division of the institute of navigation (ION GPS 1995)*, Palm Springs (pp 55–62).
Weiss, S., Achtelik, M., Lynen, S., Chli, M., & Siegwart, R. (2012). Real-time onboard visual-inertial state estimation and self-calibration of MAVs in unknown environments. In *Proceedings of the IEEE international conference on robotics and automation*. Saint Paul, MN, USA (pp. 957–964).
Wen, W., Bai, X., Kan, Y. C., & Hsu, L. T. (2019). Tightly coupled GNSS/INS integration via factor graph and aided by fish-eye camera. *IEEE Transactions on Vehicular Technology*, *68*(11), 10651–10662.
Wu, Q., Sun, M., Zhou, C., & Zhang, P. (2019). Precise point positioning using dual-frequency GNSS observations on smartphone. *Sensors, 19*(9), 2189. https://doi.org/10.3390/s19092189
Wübbena, G., Schmitz, M., & Bagg, A. (2005). PPP-RTK: Precise point positioning using state-space representation in RTK networks. In *Proceedings of the 18th international technical meeting of the satellite division of the institute of navigation (ION GNSS 2005)*. Long Beach, California, USA (pp. 2584–2594).
Yang, Y., Gao, W., Guo, S., Mao, Y., & Yang, Y. (2019). Introduction to Beidou-3 navigation satellite system. *Navigation - Journal of the Institute of Navigation, 66*(1), 7–18. https://doi.org/10.1002/navi.291
Zha, J., Zhang, B., Liu, T., & Hou, P. (2021). Ionosphere-weighted undifferenced and uncombined PPP-RTK: Theoretical models and experimental results. *GPS Solutions, 25*(4), 1–12. https://doi.org/10.1007/s10291-021-01169-0
Zhang, X., & Li, X. (2012). Instantaneous re-initialization in real-time kinematic PPP with cycle slip fixing. *GPS Solutions, 16*, 315–327. https://doi.org/10.1007/s10291-011-0233-9
Zhang, B., Teunissen, P. J. G., & Odijk, D. (2011). A novel undifferenced PPP-RTK concept. *The Journal of Navigation, 64*(S1), S180–S191. https://doi.org/10.1017/S0373463311000361
Zhang, B., Chen, Y., & Yuan, Y. (2018a). PPP-RTK based on undifferenced and uncombined observations: Theoretical and practical aspects. *Journal of Geodesy, 93*(7), 1–14. https://doi.org/10.1007/s00190-018-1220-5
Zhang, X., Tao, X., Zhu, F., Shi, X., & Wang, F. (2018b). Quality assessment of GNSS observations from an android n smartphone and positioning performance analysis using time-differenced filtering approach. *GPS Solutions, 22*(3), 1–11. https://doi.org/10.1007/s10291-018-0736-8
Zhang, X., Zhu, F., Zhang, Y., Mohamed, F., & Zhou, W. (2019). The improvement in integer ambiguity resolution with INS aiding for kinematic precise point positioning. *Journal of Geodesy, 93*(3), 993–1010. https://doi.org/10.1007/s00190-018-1222-3
Zhang, B., Hou, P., Zha, J., & Liu, T. (2021). Integer-estimable FDMA model as an enabler of GLONASS PPP-RTK. *Journal of Geodesy, 95*(8), 1–21. https://doi.org/10.1007/s00190-021-01546-0
Zhang, X., Ren, X., Chen, J., Zuo, X., Mei, D., & Liu, W. (2022). Investigating GNSS PPP–RTK with external ionospheric constraints. *Satellite Navigation, 3*(1), 1–13. https://doi.org/10.1186/s43020-022-00067-1
Zheng, K., Zhang, X., Li, P., et al. (2019). Multipath extraction and mitigation for high-rate multi-GNSS precise point positioning. *Journal of Geodesy, 93*, 2037–2051. https://doi.org/10.1007/s00190-019-01300-7
Zhong, P., Ding, X., Zheng, D., & Chen, W. (2008). Adaptive wavelet transform based on cross-validation method and its application to GPS multipath mitigation. *GPS Solutions, 12*(2), 109–117. https://doi.org/10.1007/s10291-007-0071-y
Zumberge, J. F., Heflin, M. B., Jefferson, D. C., Watkins, M. M., & Webb, F. H. (1997). Precise point positioning for the efficient and robust analysis of GPS data from large networks. *Journal of Geophysical Research Atmospheres, 102*(B3), 5005–5017. https://doi.org/10.1029/96JB03860

Publisher's Note